Supplementary Information

Critical Role of Oxide Anchoring Groups in Organic Electron Transport Layers for Perovskite Solar Cell Stability

Sanggyun Kim[1], Justine S. Wagner[2], Sina Sabury[2], Jack Lawton[1], Martin Gómez-Domínguez[1], Diana K. LaFollette[1], Dwanleen E. Shen[2], Anna M. Österholm[2], Ruipeng Li[3], Carlo A. R. Perini[1], John R. Reynolds[1,2], Juan-Pablo Correa-Baena[1,2*]

[1] School of Materials Science and Engineering, Georgia Institute of Technology, Atlanta, Georgia 30332, USA.

[2] School of Chemistry and Biochemistry, Center for Organic Photonics and Electronics, Georgia Institute of Technology, Atlanta, Georgia, 30332, USA.

[3]National Synchrotron Light Source II, Brookhaven National Lab, Upton, New York, 11973, USA.

Corresponding author: JPCB jpcorrea@gatech.edu ; JRR jreynolds43@gatech.edu

ORCID:

Sanggyun Kim 0000-0002-0620-3090

Justine S. Wagner 0000-0003-4647-0449

Sina Sabury 0000-0003-0347-7405

Jack Lawton 0009-0005-4672-1430

Martín Gómez-Domínguez 0000-0002-2613-0706

Diana K. LaFollette 0000-0003-2426-4804

Dwanleen E. Shen 0000-0002-8318-898X

Anna M. Österholm 0000-0001-6621-8238

Ruipeng Li 0000-0001-8176-3138

Carlo A.R. Perini 0000-0001-7582-2234

John R. Reynolds 0000-0002-7417-4869

Juan-Pablo Correa-Baena 0000-0002-3860-1149

Experimental Methods

Monomer Synthesis

Diethyl (4-nitrophenyl)phosphonate:

A published procedure[1] was adjusted as follows: 1-iodo-4-nitrobenzene (10 g, 49.5 mmols, 1 eq.), triethylamine (20 g, 198 mmol, 4 eq.), diethyl phosphite (7.5 g, 54.5 mmol, 1.1 eq.), $Pd(PPh_3)_4$ (1.14 g, 0.99 mmol, 0.02 eq.), and 250 mL of anhydrous toluene were added under inert atmosphere to a 500 mL round bottom flask equipped with a magnetic stir bar and a reflux condenser. The mixture stirred under reflux at 120 °C for 24 hours before cooling to room temperature. The reaction was filtered, and the filtrate was concentrated in vacuo and then redissolved in ethyl acetate. The organic layer was washed with 1M HCl, 2 M NaOH, and then brine. All organic layers were collected, dried over with sodium sulfate, filtered, and concentrated in vacuo. The crude product was then purified via silica gel chromatography using 1:1 hexanes:ethyl acetate (ETOAc), 100% DCM, and then 100% EtOAc to obtain dark red oil (8.1 g, 67% yield). ^{1}H NMR (500 MHz, $CDCl_3$) δ 8.39 – 8.14 (m, 2H), 8.14 – 7.88 (m, 2H), 4.32 – 4.00 (m, 4H), 1.33 (td, J = 7.1, 0.6 Hz, 6H). ^{31}P NMR (202 MHz, $CDCl_3$) δ 15.37. ^{13}C NMR (126 MHz, $CDCl_3$) δ 150.25, 150.22, 136.53, 135.04, 133.00, 132.91, 132.11, 128.56, 128.46, 123.41, 123.29, 62.81, 62.77, 16.35, 16.30.

Diethyl (4-aminophenyl)phosphonate:

A published procedure[2] was adjusted as follows: Diethyl (4-nitrophenyl)phosphonate (4.0 g, 15.3 mmol, 1 eq.), anhydrous tin (II) chloride (11.6 g, 61.2 mmol, 4 eq.), and 100 mL of absolute ethanol were added to a 500 mL round bottom flask equipped with a magnetic stir bar. The mixture was refluxed for 12 hours and then cooled to room temperature. The mixture was concentrated in vacuo

and suspended in 2 M KOH in distilled water. A precipitate immediately formed and filtered and washed excessively with ethyl acetate. The filtrate was collected and washed with distilled water (x1) and brine (x1) and then all organics were collected dried over with sodium sulfate, filtered, and concentrated in vacuo to receive a viscous yellow oil that solidifies (2.7 g, 77% yield). ^{1}H NMR (500 MHz, DMSO) δ 7.33 (dd, *J* = 12.5, 8.5 Hz, 2H), 6.74 – 6.50 (m, 2H), 4.05 – 3.79 (m, 4H), 1.20 (t, *J* = 7.1 Hz, 6H). ^{31}P NMR (202 MHz, DMSO) δ 21.82. ^{13}C NMR (126 MHz, DMSO) δ 153.03, 153.00, 133.42, 133.33, 113.53, 113.41, 113.35, 111.78, 61.38, 61.34, 16.67, 16.62.

Molecule Synthesis

Tetraethyl ((1,3,6,8-tetraoxo-1,3,6,8-tetrahydrobenzo[lmn][3,8]phenanthroline-2,-diyl)bis(4,1-phenylene))bis(phosphonate) [NDI-(PhDEP)$_2$]:

Napthalenetetracarboxylic dianhydride (0.78 g, 2.9 mmol, 1 eq.) and 25 mL of glacial acetic acid were added to a 250 mL round bottom flask equipped with a magnetic stir bar. The reaction stirred for 10 minutes at 60 °C before diethyl P-(2-aminoethyl)phosphonate (2.0 g, 8.7 mmol, 3 eq.) was added. The temperature was raised to 90 °C and the reaction was left to stir for 48 hours. Afterwards, the reaction cooled to room temperature before precipitating into cold distilled water. The precipitate was filtered and washed excessively with distilled water. The filtered powder was then placed under high vacuum to dry for 24 hours and then purified via silica gel chromatography using 100% DCM to 20% MeOH in DCM to obtain a light brown powder (1.13 g, 50% yield). ^{1}H NMR (500 MHz, $CDCl_3$) δ 8.89 (s, 4H), 8.07 (dd, *J* = 13.0, 8.4 Hz, 4H), 7.57 – 7.41 (m, 4H), 4.38 – 4.09 (m, 8H), 1.41 (t, *J* = 7.1 Hz, 12H). ^{31}P NMR (202 MHz, $CDCl_3$) δ 17.67. ^{13}C NMR (126 MHz, $CDCl_3$) δ 162.63, 153.89, 138.14, 133.19, 133.10, 131.66, 128.91, 128.78, 126.96, 62.47, 62.43, 32.44, 16.43, 16.38.

((1,3,6,8-tetraoxo-1,3,6,8-tetrahydrobenzo[lmn][3,8]phenanthroline-2,-diyl)bis(4,1-phenylene))bis(phosphonic acid) [NDI-(PhPA)$_2$]:

Tetraethyl((1,3,6,8-tetraoxo-1,3,6,8-tetrahydrobenzo[lmn][3,8]phenanthroline-2,-diyl)bis(4,1-phenylene))bis(phosphonate) (0.8 g, 1.2 mmol, 1 eq.) and 25 mL of anhydrous dichloromethane were added to a 100 mL round bottom flask equipped with a magnetic stir bar under an inert atmosphere. After stirring for 10 minutes at room temperature, bromotrimethylsilane (1.8 g, 11.6 mmol, 10 eq.) was added and the reaction was left to stir overnight at room temperature. After 12 hours, 3 mL of methanol was added, and the mixture was left to stir for an additional 3 hours. The solution was then concentrated to complete dryness and the powder was suspended in methanol and filtered. The product was then dried under high vacuum to receive a light tan/brown powder (0.7 g, 100% yield). ^{1}H NMR (500 MHz, DMSO) δ 8.74 (s, 4H), 7.97 – 7.77 (m, 4H), 7.68 – 7.47 (m, 4H), 3.17 (s, 4H).^{31}P NMR (202 MHz, DMSO) δ 12.30. ^{13}C NMR (126 MHz, DMSO) δ 163.39, 138.39, 131.82, 131.73, 130.95, 129.45, 139.33, 127.49, 127.22, 107.35, 49.07.

2,7-bis(4-bromphenyl)benzo[lmn][3,8]phenanthroline-1,3,6,8(2H,7H)-tetraone [NDI-(PhBr$_2$]:

Napthalenetetracarboxylic dianhydride (6.0 g, 22.4 mmol, 1 eq.) and 4-bromoaniline (9.6 g, 55.9 mmol, 2.5 eq.) and 100 mL of anhydrous dimethylformamide were added to a round bottom flask equipped with a stir bar. The reaction mixture was placed on a hot plate at 120 °C and left to stir overnight. Afterwards, the reaction cooled to room temperature, was filtered, and washed with methanol to obtain a yellow powder. ^{1}H NMR (500 MHz, DMSO) δ 8.74 (s, 4H), 7.79 (d, J = 8.5 Hz, 4H), 7.46 (d, J = 8.5 Hz, 4H). ^{13}C could not be obtained due to limited solubility and low resolution. ESI-MS: m/z theoretical 574.9236, obtained 574.9240.

Perovskite Solar Cell (PSC) Fabrication

Patterned fluorine-doped tin oxide (FTO) glass substrates (7 Ω/sq) were sequentially cleaned by ultrasonication for 15 min in 2% Mucasol (Schülke) solution, deionized water, acetone (≥ 99.5%, Sigma-Aldrich), and isopropyl alcohol (IPA, 99.9%, Fisher Chemical). The cleaned substrates were then dried with N_2 gun and subjected to UV-ozone treatment for 15 min. For the electron transport layer (ETL), a compact TiO_2 (c-TiO_2) layer was deposited via spray pyrolysis using a precursor solution composed of 800 µL titanium diisopropoxide bis(acetylacetonate) 75 wt.% in IPA (Sigma-Aldrich) and 10.8 mL ethanol (anhydrous, ≥ 99.5%, Sigma-Aldrich). The solution was sprayed onto preheated substrates at 450 °C in cycles, with 30 s interval between each cycle, followed by post-annealing at 450 °C for 30 min. Easy spray cycle lasted 16–18 s, with O_2 supplied as a carrier gas at a flow rate of 3 L min^{-1}. After cooling to room temperature, a 60 µL 150 mg mL^{-1} mesoporous TiO_2 (mp-TiO_2) solution was spin-coated statically at 4000 rpm for 10 s (acceleration: 4000 rpm s^{-1}). The mp-TiO_2 solution was prepared by diluting TiO_2 paste (Sigma-Aldrich) in anhydrous in anhydrous ethanol (≥ 99.5%, Sigma-Aldrich). The mp-TiO_2 coated substrates were then dried at 100 °C for 10 min and sintered at 450 °C for 30 min.

NDI-$(PhPA)_2$ and NDI-$(PhBr)_2$ ETL thin films were fabricated using chemical bath deposition (CBD) method. The cleaned patterned FTO substrates were treated in UV-ozone for 1 hour and then immersed in a pre-heated 0.5 mg mL^{-1} solution of NDI-based ETL molecules in dimethyl sulfoxide (DMSO, Sigma-Aldrich, ≥ 99.8%) at 100°C for varying durations, maintaining a constant temperature throughout the process. Following CBD, the substrates were rinsed by dipping them in ethanol (EtOH) three times, and then annealed at 120 °C for 10 min. All ETL

depositions steps were conducted in ambient air, and the substrates were subsequently transferred to an N_2 filled glove box (O_2 and H_2O < 4 ppm).

The $Cs_{0.09}FA_{0.91}PbI_3$ (CsFA) perovskite film was deposited via a two-step spin-coating process using a 1.2 M precursor solution with 5% excess Pb, prepared by dissolving cesium iodide (Sigma-Aldrich), formamidinium iodide (GreatCell Solar), and lead iodide (Tokyo Chemical Industry, > 98%) in a 2:1 (v/v) mixture of N,N-dimethylformamide (DMF, Sigma-Aldrich, ≥ 99.8%) and DMSO. A 90 µL CsFA solution was spin-coated at 1000 rpm for 10 s (acceleration: 1000 rpm s^{-1}), followed by 6000 rpm for 20 s (acceleration: 6000 rpm s^{-1}), ensuring uniform solution spreading prior to spin coating. Three seconds before the end of the second step, 250 µL of chlorobenzene (Sigma-Aldrich, 99%) was continuously dispensed onto the substrate during spin coating, and the CsFA film was annealed at 150 °C for 10 min. Next, a 90 µL of phenethyl ammonium iodide (PEAI, Dyenamo) solution at 1 mg mL^{-1} in IPA (Sigma-Aldrich, anhydrous, 99.9%), was spin coated on top of CsFA film at 5000 rpm for 20 s (acceleration: 5000 rpm s^{-1}).

For the hole transport layer (HTL), a 90 µL doped Spiro-OMeTAD solution was spin-coated statically at 3000 rpm for 30 s (acceleration: 3000 rpm s^{-1}). A doped Spiro-OMeTAD solution was prepared by dissolving Spiro-OMeTAD (1-Material) in 0.07 M chlorobenzene (Sigma-Aldrich, 99.9%), followed by the sequential addition of 0.4 mol-to-mol lithium bis(trifluoromethane)sulfonimide (Li-TFSI, Sigma-Aldrich) in 1.8 M acetonitrile (Sigma-Aldrich, anhydrous, 99.8%), 3.3 mol-to-mol 4-tertbutylpyridine (tBP, Sigma-Aldrich, 98%), and 0.03 mol-to-mol tris(2-(1H-pyrazol-1-yl)-4-tert-butylpyridine)cobalt(III) tri[bis(trifluoromethane)sulfonimide] (FK 209 Co (III), Sigma-Aldrich) in 0.25 M acetonitrile.

From CsFA film to HTL processing, all steps were performed inside N_2 filled glove box (O_2 and H_2O < 4 ppm) at a controlled temperature of 18 °C to 24 °C. The edges of the substrates were cleaned in ambient air using DMF, followed by acetonitrile, to remove CsFA film and HTL. Finally, a 50 nm Au metal contact (Kurt J. Lesker, 99.999%) was thermally evaporated through a shadow mask, forming 8 independent cells per substrate. The active device area is 0.128 cm^2.

Characterization

^{1}H, ^{13}C, and ^{31}P Nuclear Magnetic Resonance (NMR):

NMR spectra for all monomers and molecular precursors were acquired through Bruker Avance IIIHD 500 MHz or Bruker Avance IIIHD 700 MHz instruments using $CDCl_3$ or DMSO-d6 as solvent; the residual $CHCl_3$ peak was used as a reference for all reported chemical shifts (^{1}H: δ= 7.26 ppm, ^{13}C: δ= 77.16 ppm). For ^{31}P NMR spectra, 85% H_3PO_4 was used as the external reference.

Thermogravimetric Analysis (TGA):

TGA was performed using a Mettler Toledo TGA2 STAR System Thermogravimetric Analyzer. 5 mg of molecules were heated from 50 °C to 700 or 900 °C at a temperature rate of 15 °C min^{-1} in a N_2 rich atmosphere.

Ultraviolet-visible (UV-Vis) Spectroscopy:

Absorption, transmittance, and reflectance spectra were measured using Cary 5000 UV-Vis NIR spectrophotometer. A double-beam configuration was employed to account for the optical influence of the glass substrate, ensuring accurate measurements for the NDI-based molecular films. For solution UV-Vis, solution concentration was 0.02 mg mL^{-1} NDI-based ETL molecules in DMSO.

X-ray Photoelectron Spectroscopy (XPS):

XPS analysis was conducted using a Thermo Scientific K-Alpha system equipped with a monochromatic Al Kα X-ray source (hv = 1486.6 eV). The incident X-ray beam was aligned at 60° relative to the sample normal, while photoelectrons were collected at 0° emission angle. All spectra were acquired under high vacuum conditions with the chamber pressure maintained below 1×10^{-7} Torr. Both survey and high-resolution scans were obtained. Survey spectra were averaged over two measurements with 200 eV pass energy, 50 ms dwell time, and 0.1 eV step size. High-resolution scans were averaged over 20 measurements for C 1s, Br 3d, P 2p, and O1s, while 10 measurements were used for N 1s, S 2p, and Cl 2p, and 5 measurements for Sn 3d. Peak fitting was conducted using the Thermo Scientific Advantage Data System. To correct for potential surface charging effects, all binding energies were referenced to the C-C (284.8 eV) peak position.

Scanning Electron Microscopy (SEM):

SEM imaging was performed using a Hitachi SU8230 with a secondary electron detector, operation at 5 kV accelerating voltage and an emission current of 10 mA.

Contact Angle (CA):

CA measurements were conducted using ramé-hart (Model 290) and analyzed through Image J software via low bond axisymmetric drop shape analysis. To evaluate the surface polarity, 2.5 μL deionized water (polar) was deposited onto the surface of interest.

Grazing Incidence Wide-Angle X-ray Scattering (GIWAXS):

Synchrotron GIWAXS measurements were carried out at beamline 11-BM of the National Synchrotron Light Source II (NSLS-II) at Brookhaven National Laboratory. The X-ray beam had an energy of 13.5 keV and a spot size of 0.2 mm × 0.05 mm. Samples were irradiated for 10

seconds at incident angles of 0.05°, 0.1°, and 0.5°. The beam divergence was 1 mrad, with an energy resolution of 0.7%. Data processing and analysis were performed using the SciAnalysis software package provided by the beamline.

PSC Device Characterization:

The photovoltaic performance of the devices was assessed using a Fluxim Litos Lite system equipped with a Wavelabs Sinus-70 AAA solar simulator, providing AM 1.5G illumination at room temperature under ambient conditions. Current-density-voltage (J-V) characteristics were recorded in both forward and reverse scan directions, sweeping from 1.2 V to -0.5 V at a scan rate of 50 mV s^{-1}. Maximum power point tracking (MPPT) was employed to determine the stabilized power output over a 120-second period. A mask was utilized to define the cell area of 0.0625 cm^2, while the total active device area remained 0.128 cm^2. During measurements, N_2 gas flow was introduced, but temperature control was not implemented. No pre-condition treatments, such as light-soaking or applied bias voltage, were performed prior to testing.

For long-term stability analysis, a Fluxim Litos stress-test platform was used to evaluate device degradation. The PSCs were exposed to 1 sun equivalent illumination (UV-filtered) in an N_2-rich atmosphere at 25°C or 65°C while continuously operating under MPPT conditions. Stability measurement followed the International Summit on Organic PV Stability (ISOS) L-1I and L-2I protocols, where L, 1, 2, I represent light exposure under bias, room temperature operation, elevated temperature conditions, and an inert atmosphere, respectively[3]. To monitor performance degradation, automated *J-V* scans in both reverse and forward directions were acquired every 12 hours thought the stability test. A mask was not applied, and measurements were based on the total active device area of 0.128 cm^2.

Supplementary Note 1

To examine the influence of molecular coverage on long-term stability, PSCs incorporating NDI-$(PhPA)_2$ and NDI-$(PhBr)_2$ with a 24-hour CBD process were also tested under ISOS-L-1I conditions (**Fig. S24-S25**). These devices initially exhibited maximum reverse scan PCEs of 14.02% (median 10.49%) for NDI-$(PhPA)_2$ and 15.69% (median 12.50%) for NDI-$(PhBr)_2$ (**Fig. S23**, **Table S3**). The NDI-$(PhPA)_2$ devices demonstrated linear degradation trends, indicating that sufficient molecular coverage is critical for maintaining light stability in PSC. On the other hand, devices treated with NDI-$(PhBr)_2$ displayed abrupt performance losses, mirroring trends observed in the 72-hour CBD process. These findings further align with prior observations that anchoring groups enhance molecular adhesion and durability with proper coverage, ultimately influencing PSC longevity and performance.

The relationship between molecular coverage and interfacial properties was further supported by CA measurements on FTO processed using the optimized 72-hour CBD process with NDI-$(PhPA)_2$ and NDI-$(PhBr)_2$. NDI-$(PhPA)_2$ thin films exhibited a lower and more consistent water contact angle (41.74° ± 0.33°) compared to NDI-$(PhBr)_2$ (47.29° ± 11.87°), indicating superior wettability for perovskite precursor solutions (**Fig. S27**). The stronger coordination of the phosphonic acid groups with the FTO surface results in a more uniform, hydrophilic interface relative to FTO water contact angle of (55.20° ± 1.89°). The larger variation in water contact angles observed on NDI-$(PhBr)_2$ treated FTO is likely a result of the CBD process itself, as NDI-$(PhBr)_2$ is not retained on the FTO surface.

PSCs incorporating NDI-$(PhPA)_2$ and NDI-$(PhBr)_2$ without the EtOH dipping step (referred to as "excess" conditions) were subjected to ISOS-L-2I testing (**Fig. S26**) to understand the impact of unbound molecules on perovskite phase stability as shown in our previous work with phosphonic acids.[4] The maximum reverse scan PCEs were 13.57% (median 11.5%) for NDI-$(PhPA)_2$ excess and 12.77% (median 11.54%) for NDI-$(PhBr)_2$ excess; full photovoltaic parameters are reported in **Figure S23** and **Table S3**. Unlike NDI-$(PhPA)_2$ excess, the NDI-$(PhBr)_2$ excess devices exhibited further reductions in stabilized PCE, suggesting that residual NDI-$(PhBr)_2$ molecules disrupt the interfacial environment. However, under ISOS-L-2I thermal stress testing, NDI-$(PhPA)_2$ excess showed accelerated degradation, highlighting the detrimental impact of unbound molecules, while NDI-$(PhBr)_2$ excess devices were even less stable than without ETL devices.

XPS measurements were also conducted on NDI-$(PhPA)_2$ excess and NDI-$(PhBr)_2$ excess thin films (**Fig. S27**). The P 2p spectrum of NDI-$(PhPA)_2$ excess displayed an identical peak at 133.5 eV, consistent with that observed for the NDI-$(PhPA)_2$ thin film. Nonetheless, NDI-$(PhBr)_2$ excess film showed two distinct Br 3d peaks appeared at 70.6 eV and 71.5 eV, features absent in EtOH dipped samples. This indicates that, in the absence of the EtOH dip, residual NDI-$(PhBr)_2$ molecules remain on the surface and likely engage in different interactions with the FTO substrate. Furthermore, N 1s signals at 400.8 eV were observed for both NDI-$(PhPA)_2$ excess and NDI-$(PhBr)_2$ excess, with greater intensity for NDI-$(PhPA)_2$ excess films, suggesting a higher degree of molecular retention relative to NDI-$(PhBr)_2$.

SEM analysis was performed to assess how PhPA and PhBr functional groups on NDI-derivatives influence perovskite film morphology for the 24-hour CBD process (**Fig. S28**).

Although it was initially hypothesized that the more hydrophilic surface provided by NDI-$(PhPA)_2$ could reduce perovskite grain sizes and increase grain boundary density, potentially contributing to open-circuit voltage (V_{OC}) losses[5], SEM images revealed no significant differences in grain size across perovskite films deposited on NDI-$(PhPA)_2$, NDI-$(PhBr)_2$, and their excess conditions. This suggests that observed reduction in V_{OC} is likely attributed to change in the work function of the FTO induced by the presence of NDI-$(PhPA)_2$ interlayer. To further probe structural impacts, GIWAXS measurements were conducted on perovskite films deposited atop NDI-$(PhPA)_2$ excess and NDI-$(PhBr)_2$ excess layers. The GIWAXS data also revealed no notable changes in crystalline structure compared to perovskite films deposited on conventional c-TiO_2 + mp-TiO_2 layer, indicating that the presence of excess molecules does not alter the crystalline structures of the perovskite layer (**Fig. S29**). Moreover, cross-sectional SEM images of REF, w/o ETL, and 72-hour CBD-processed NDI-$(PhPA)_2$ PSCs showed comparable perovskite grain sizes across all devices (**Fig. S31**).

Figures & Tables

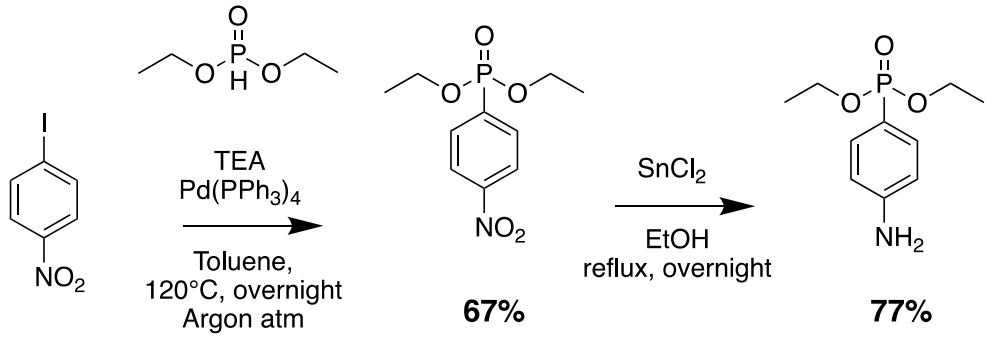

Figure S1. Monomer synthesis scheme for diethyl (4-aminophenyl)phosphonate.

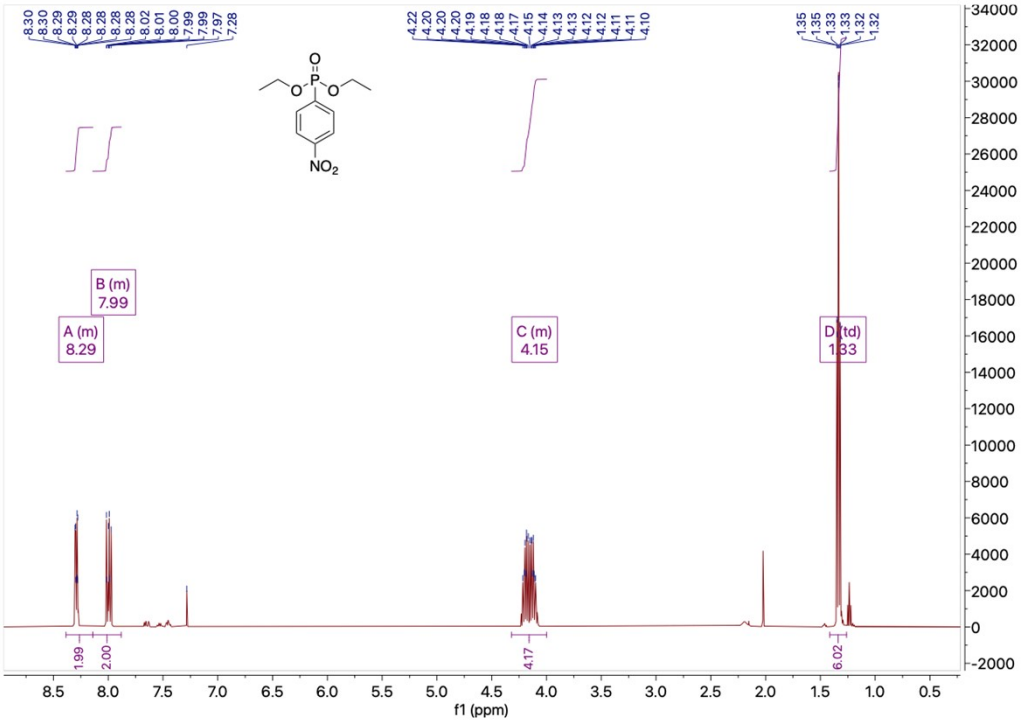

Figure S2. ^{1}H NMR spectrum of diethyl (4-nitrophenyl)phosphonate.

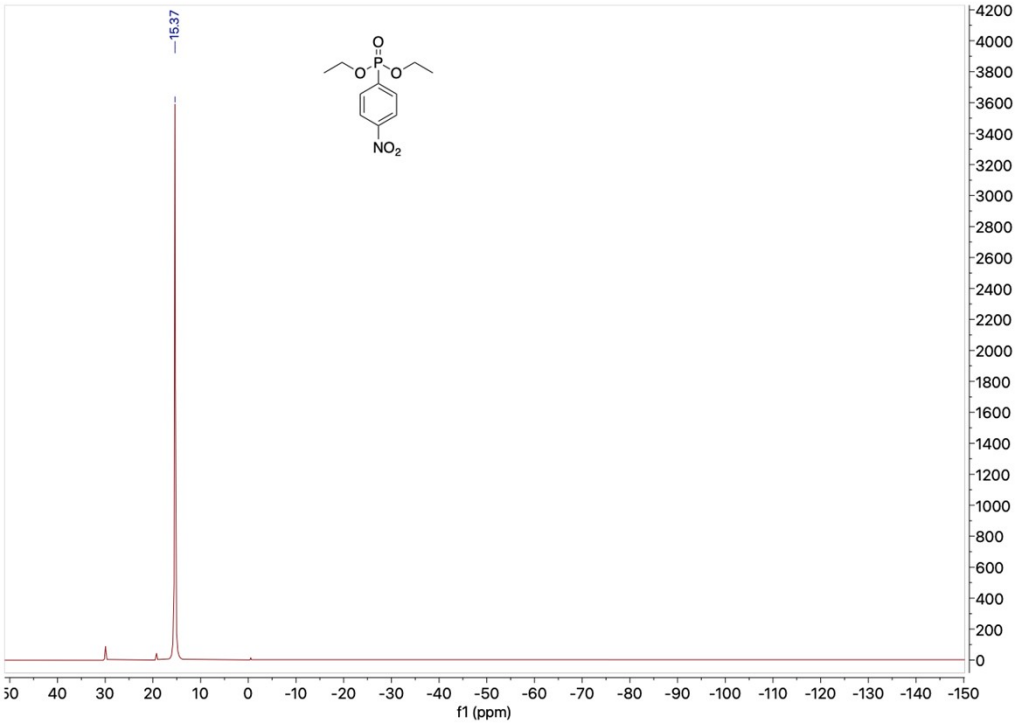

Figure S3. ^{31}P NMR spectrum of diethyl (4-nitrophenyl)phosphonate.

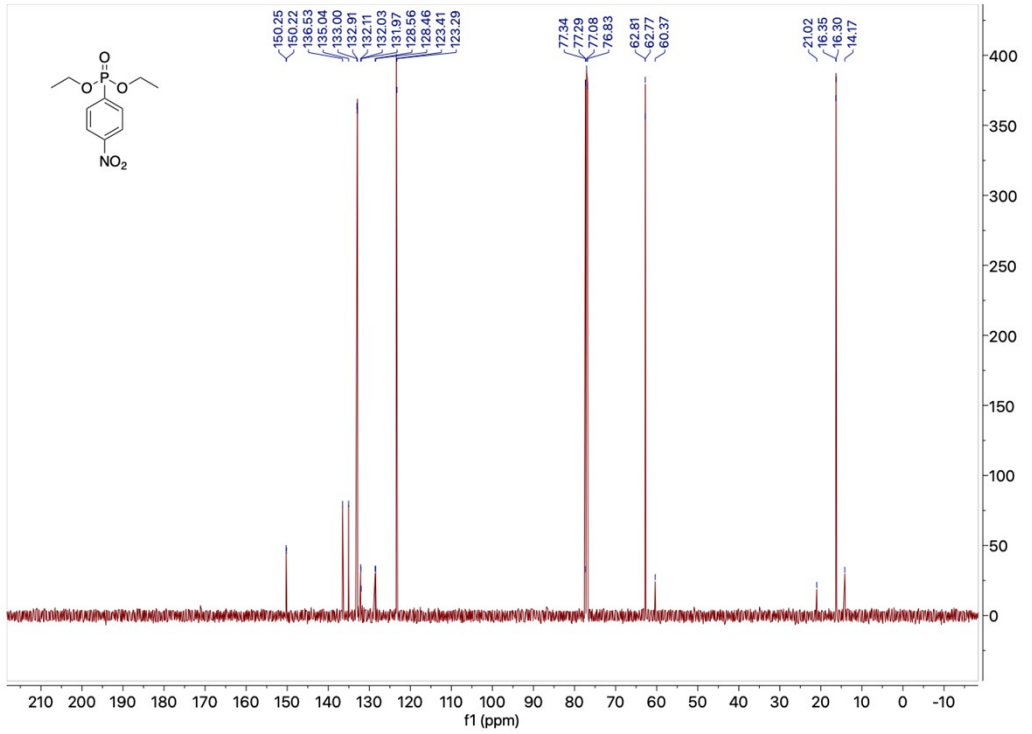

Figure S4. ^{13}C NMR spectrum of diethyl (4-nitrophenyl)phosphonate.

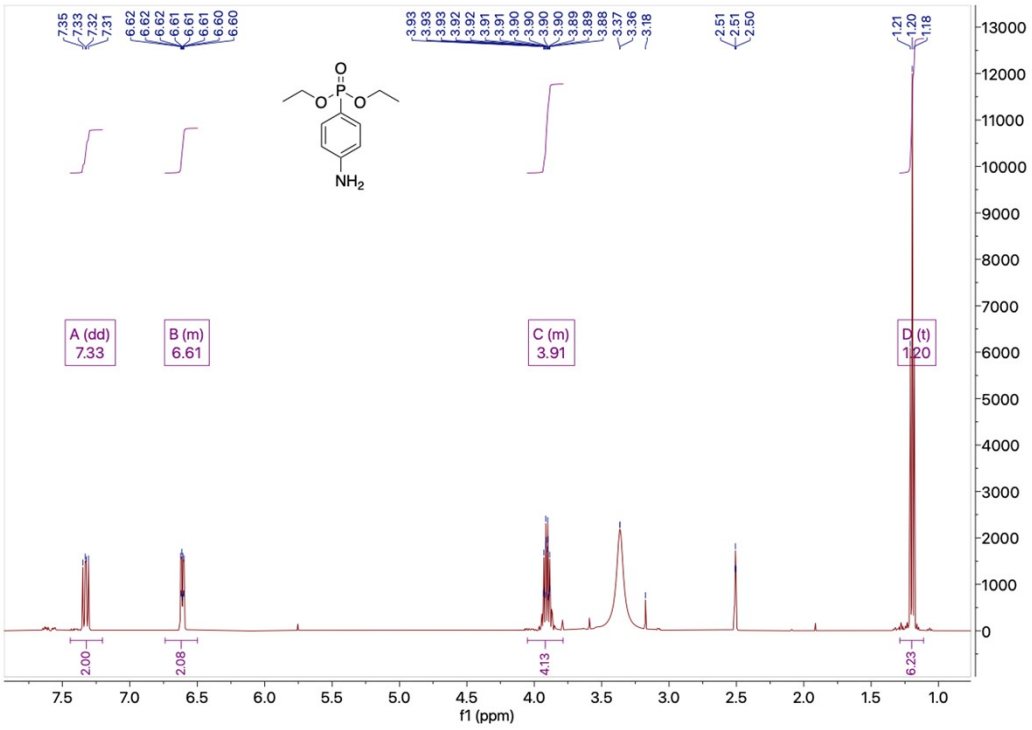

Figure S5. ^{1}H NMR spectrum of diethyl (4-aminophenyl)phosphonate.

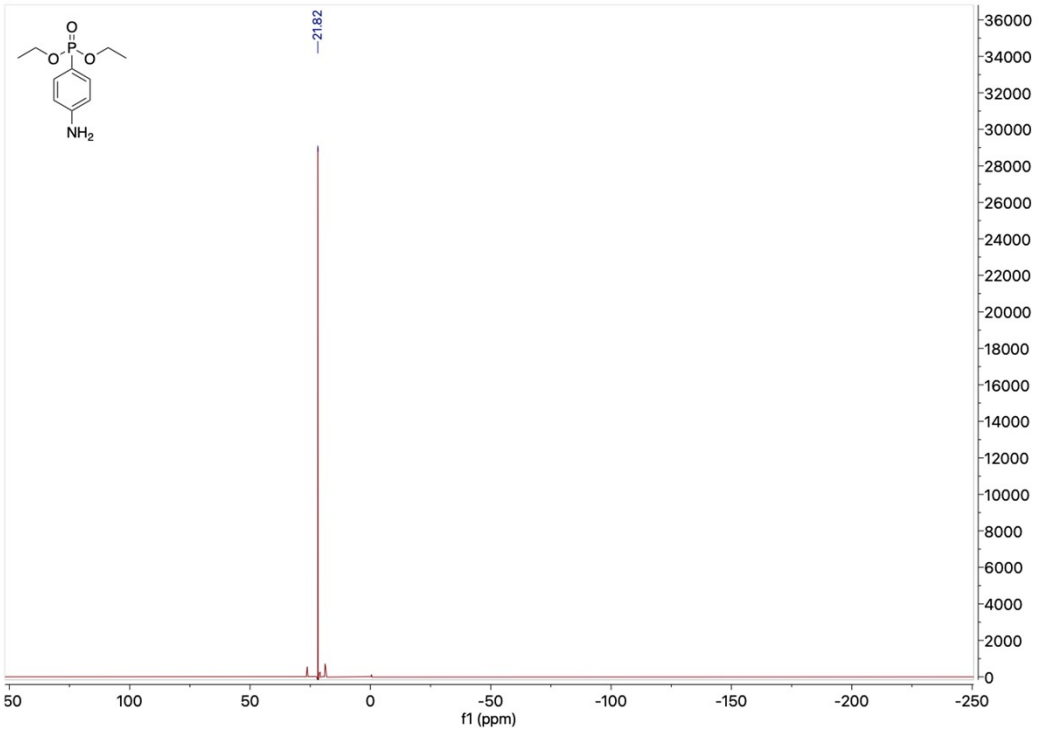

Figure S6. ^{31}P NMR spectrum of diethyl (4-aminophenyl)phosphonate.

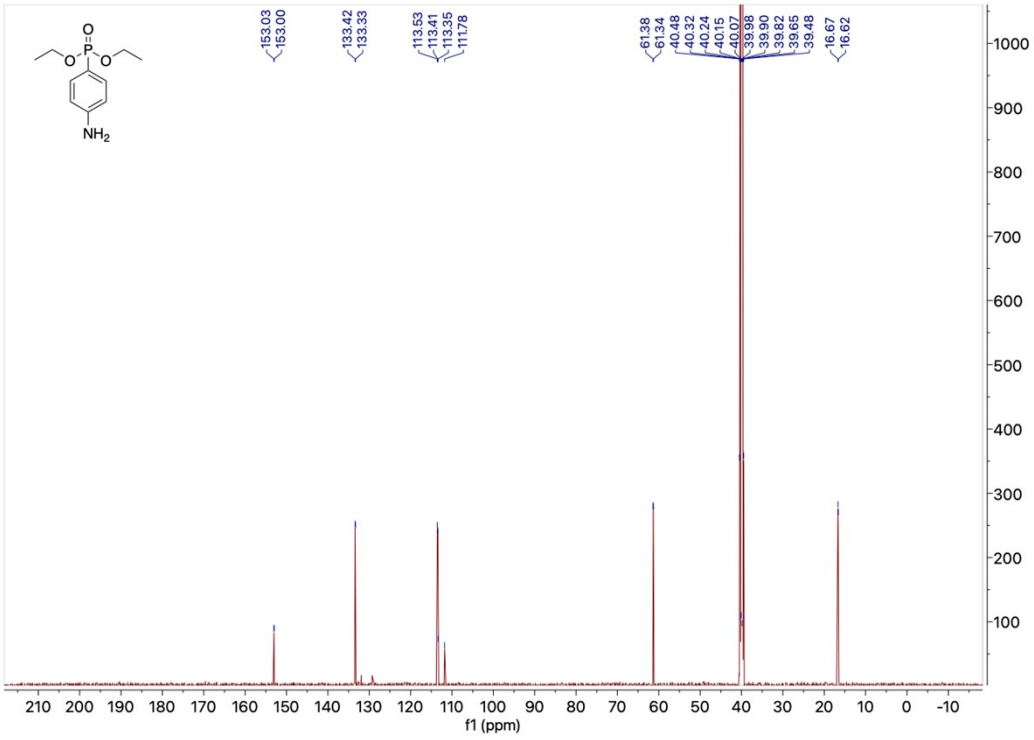

Figure S7. ^{13}C NMR of diethyl (4-aminophenyl)phosphonate.

1) NDI-(PhPA)$_2$ Synthesis:

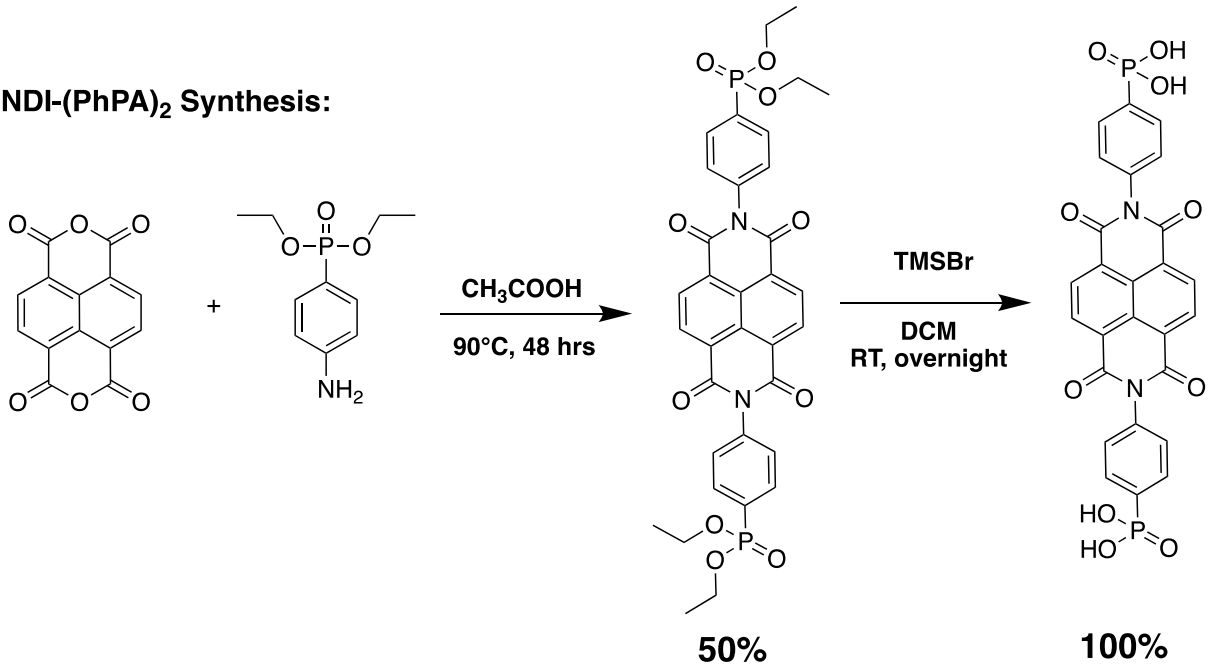

2) NDI-(PhBr)$_2$ Synthesis:

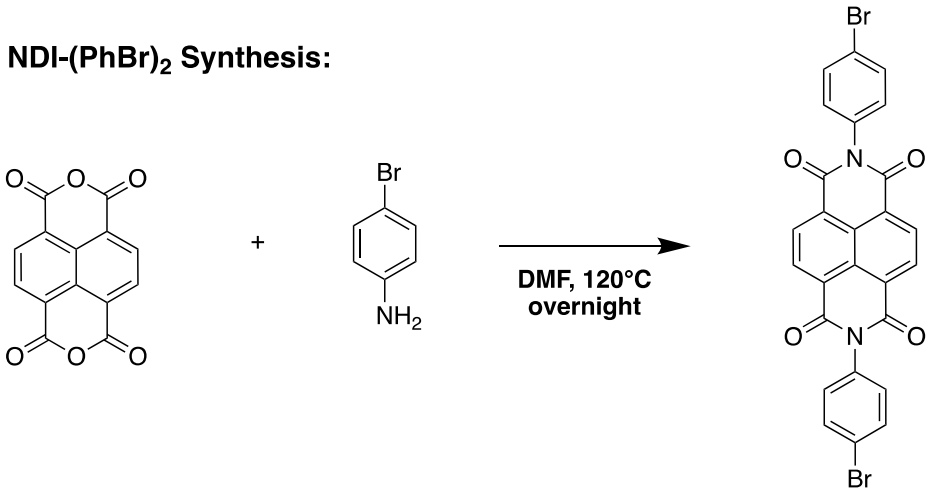

Figure S8. Synthetic scheme for NDI-(PhPA)$_2$ and NDI-(PhBr)$_2$.

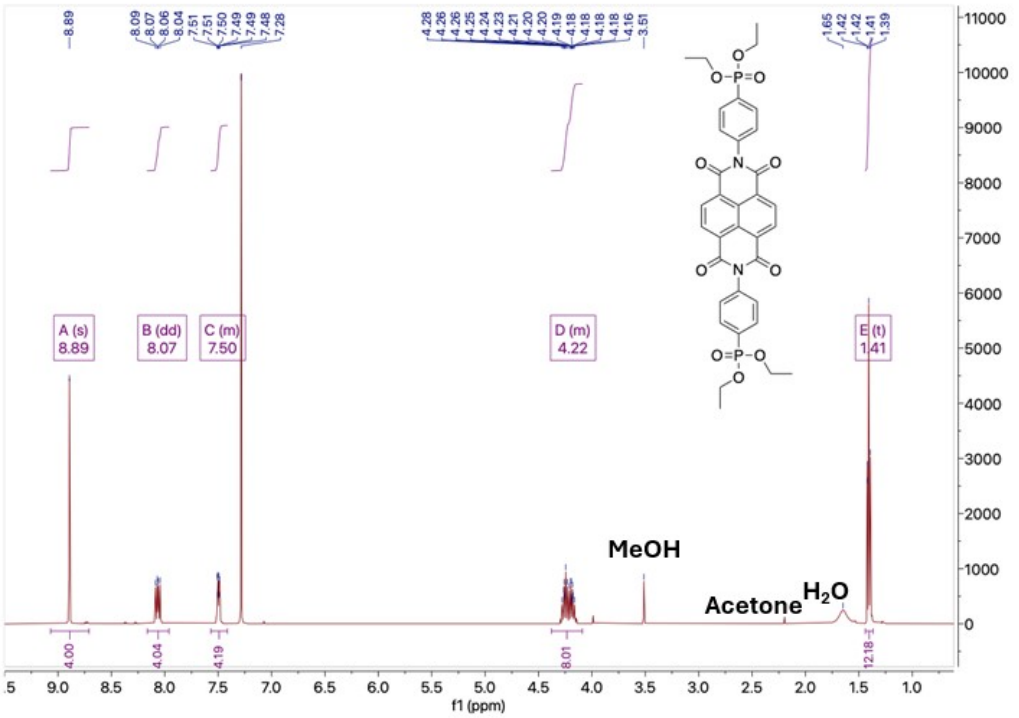

Figure S9. ^{1}H NMR spectrum of NDI-$(PhDEP)_2$.

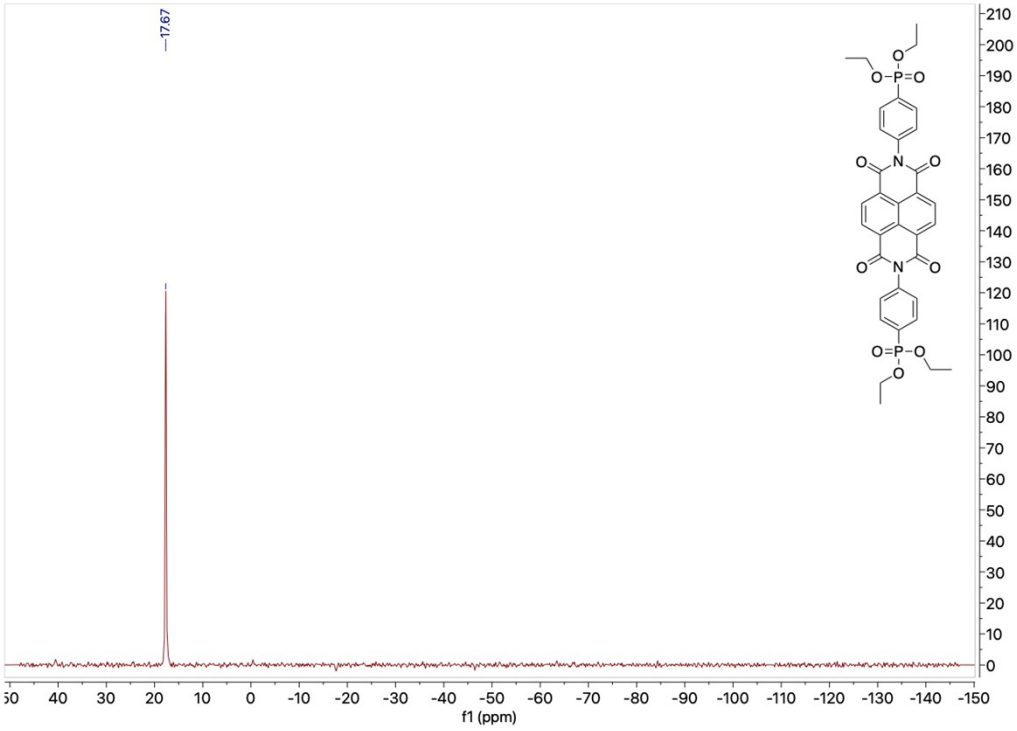

Figure S10. ^{31}P NMR spectrum of NDI-$(PhDEP)_2$.

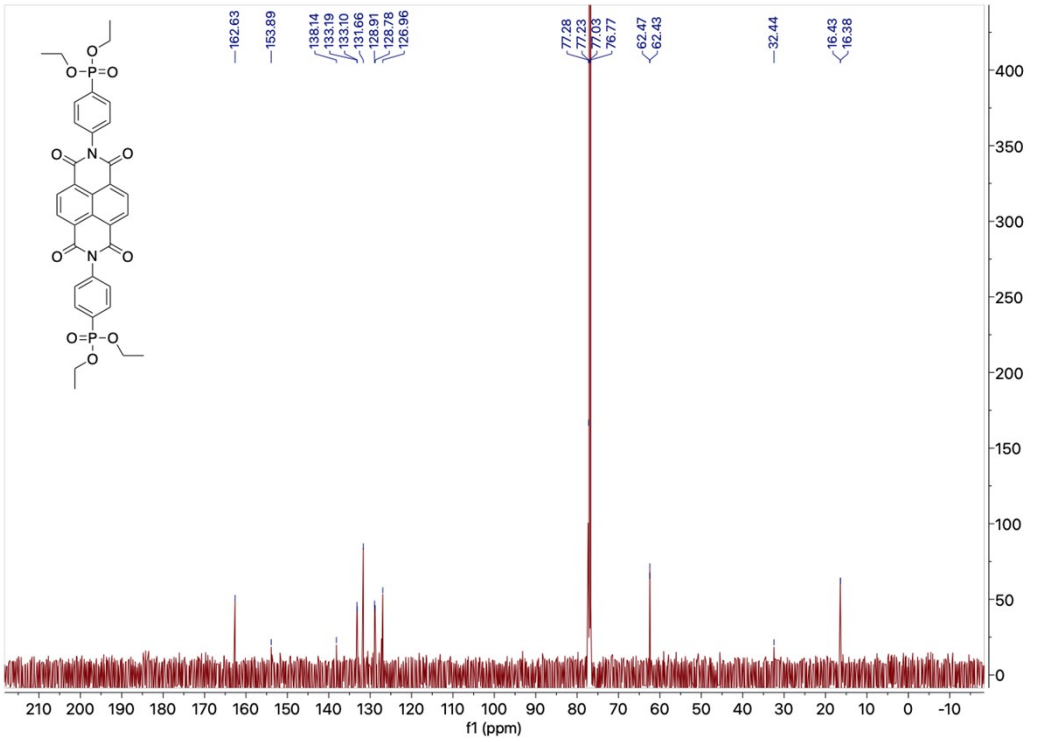

Figure S11. ^{13}C NMR of NDI-$(PhDEP)_2$.

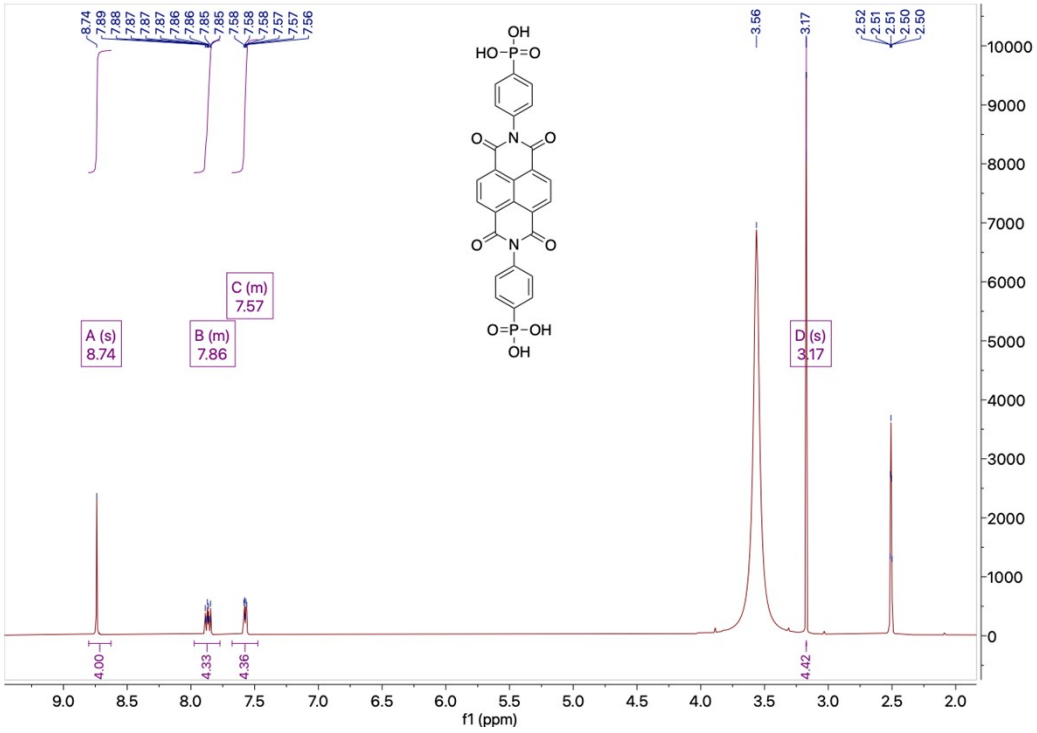

Figure S12. ^{1}H NMR spectrum of NDI-$(PhPA)_2$. The peak at 3.6 ppm originates from residual H_2O.

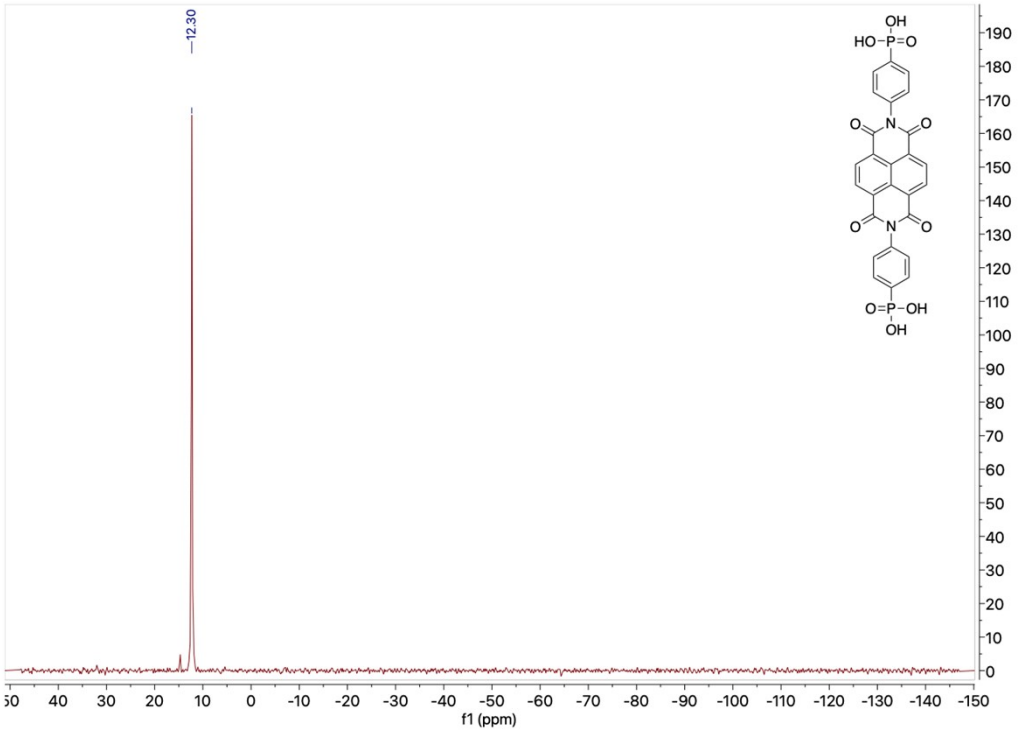

Figure S13. ^{31}P NMR spectrum of NDI-$(PhPA)_2$.

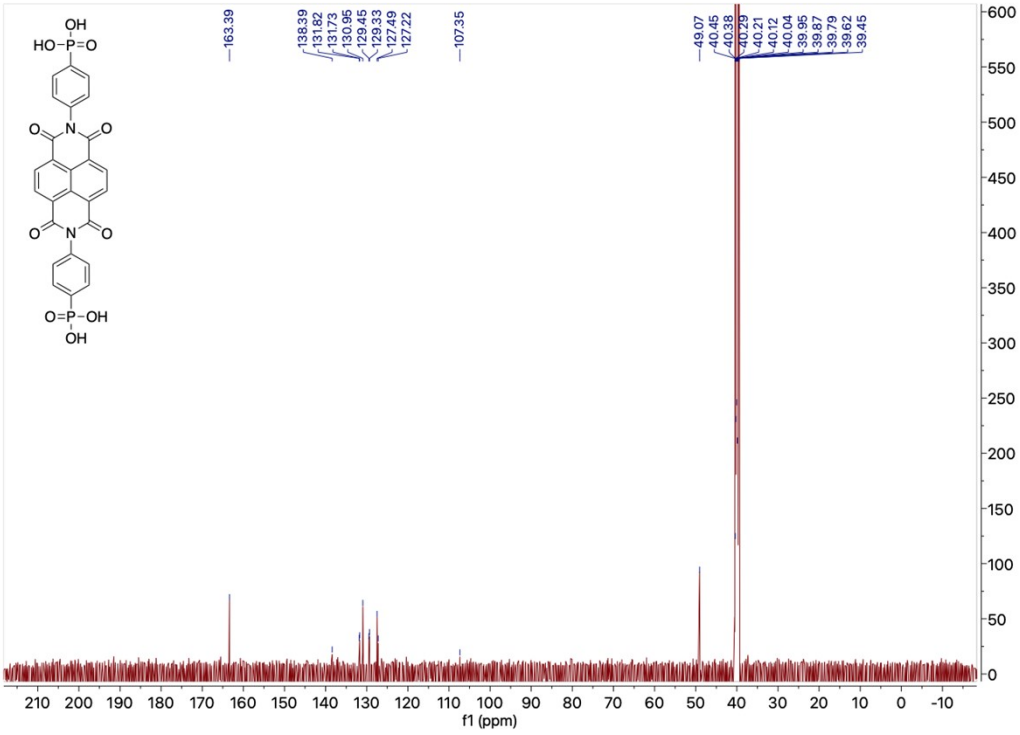

Figure S14. ^{13}C NMR spectrum of NDI-$(PhPA)_2$.

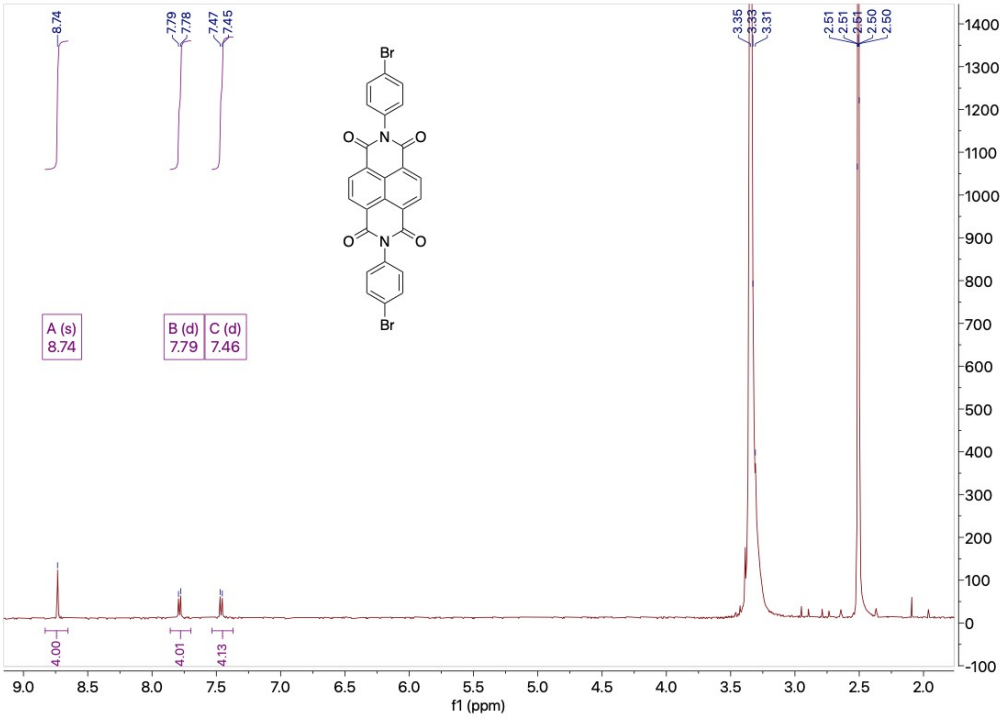

Figure S15. ^{1}H NMR spectrum of NDI-$(PhBr)_2$. The peak at 3.6 ppm originates from residual H_2O.

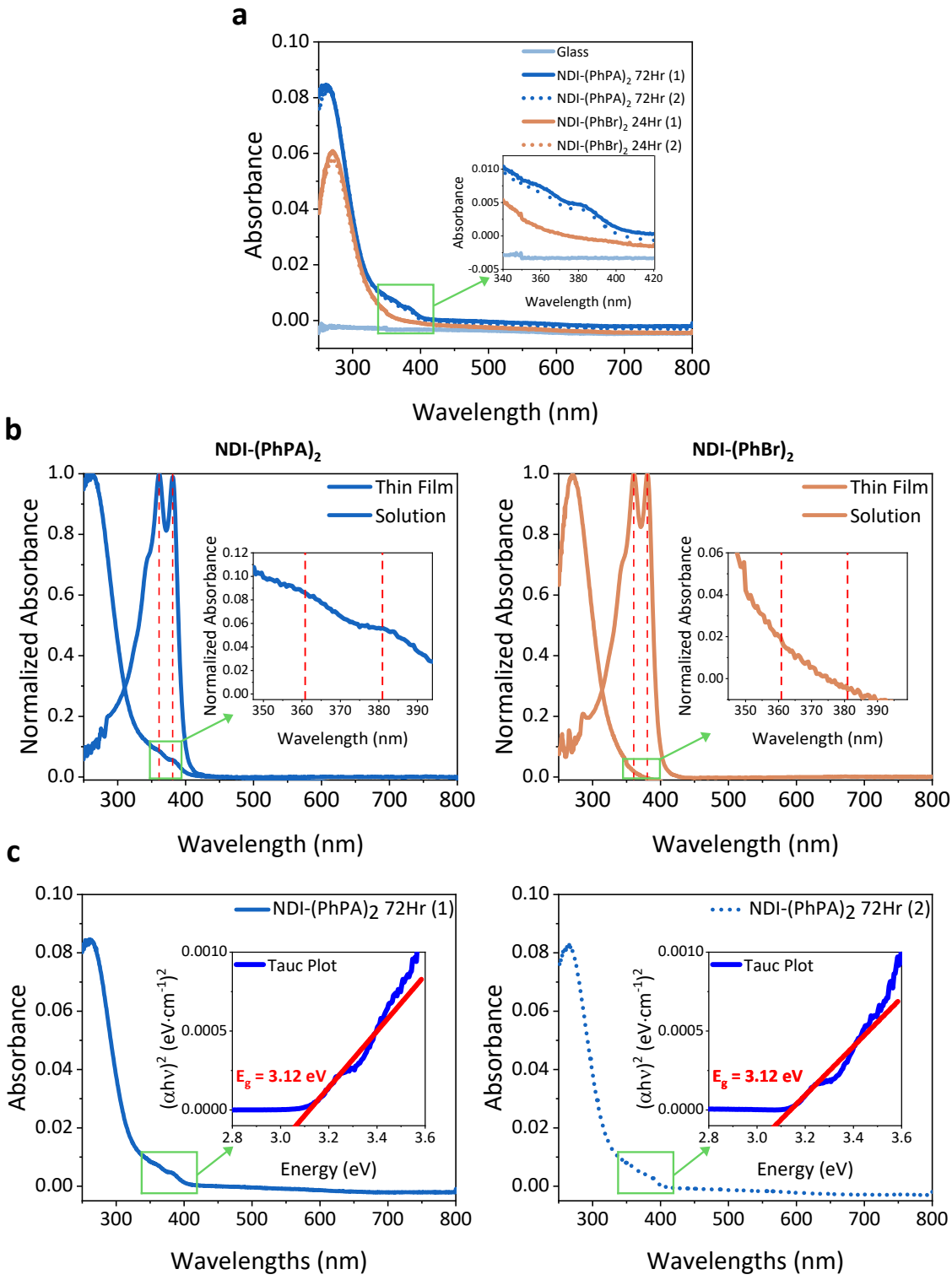

Figure S16. UV-Vis absorption spectra of NDI-based ETL (a) thin films and (b) solution in DMSO. (c) Optical HOMO-LUMO gap determination of NDI-$(PhPA)_2$ thin films using Tauc method. The red dashed lines indicate the maximum absorption peak observed in the solution UV-Vis spectrum of the corresponding molecule.

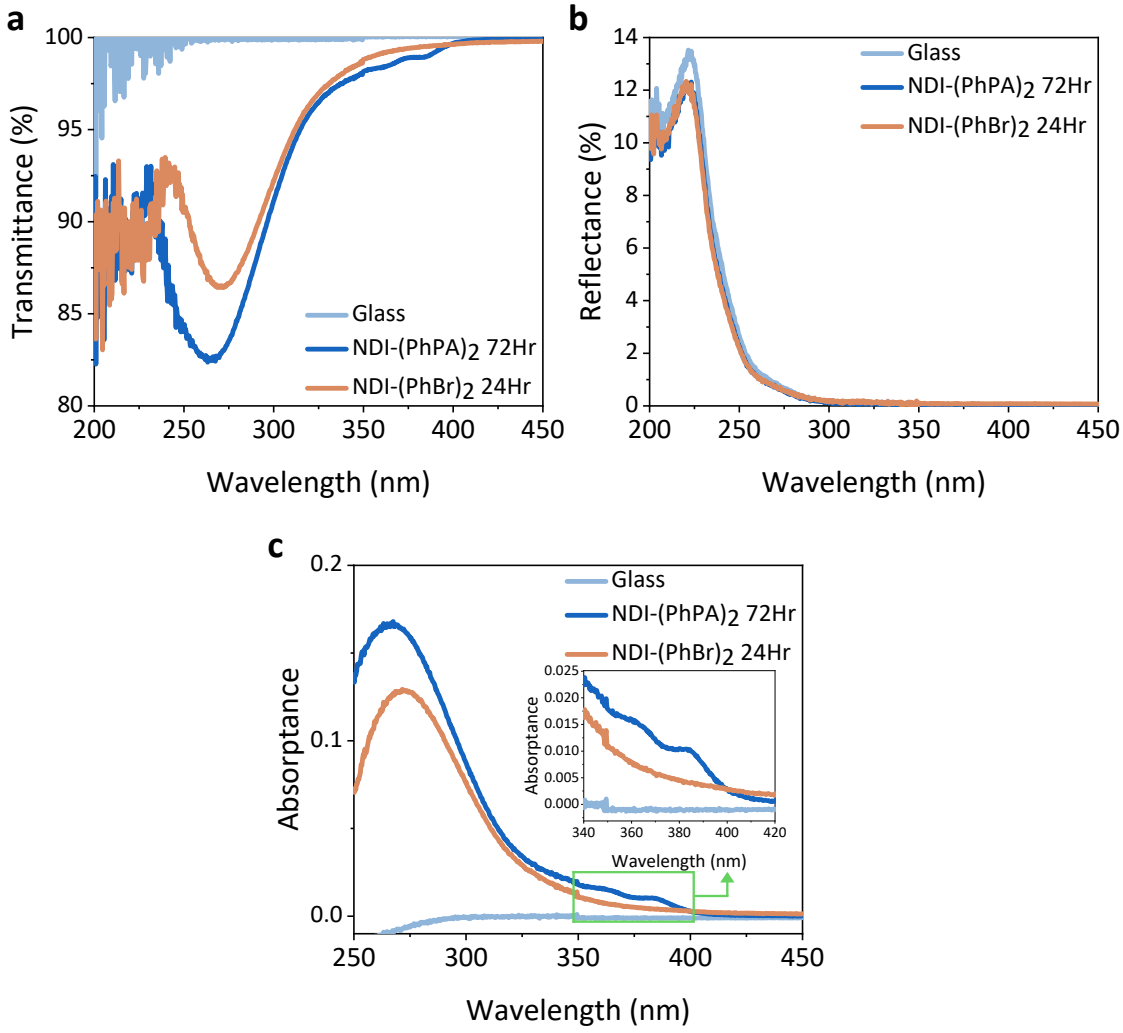

Figure S17. (a) Reflectance, (b) transmittance, and (c) absorptance spectra of NDI-based ETL thin films.

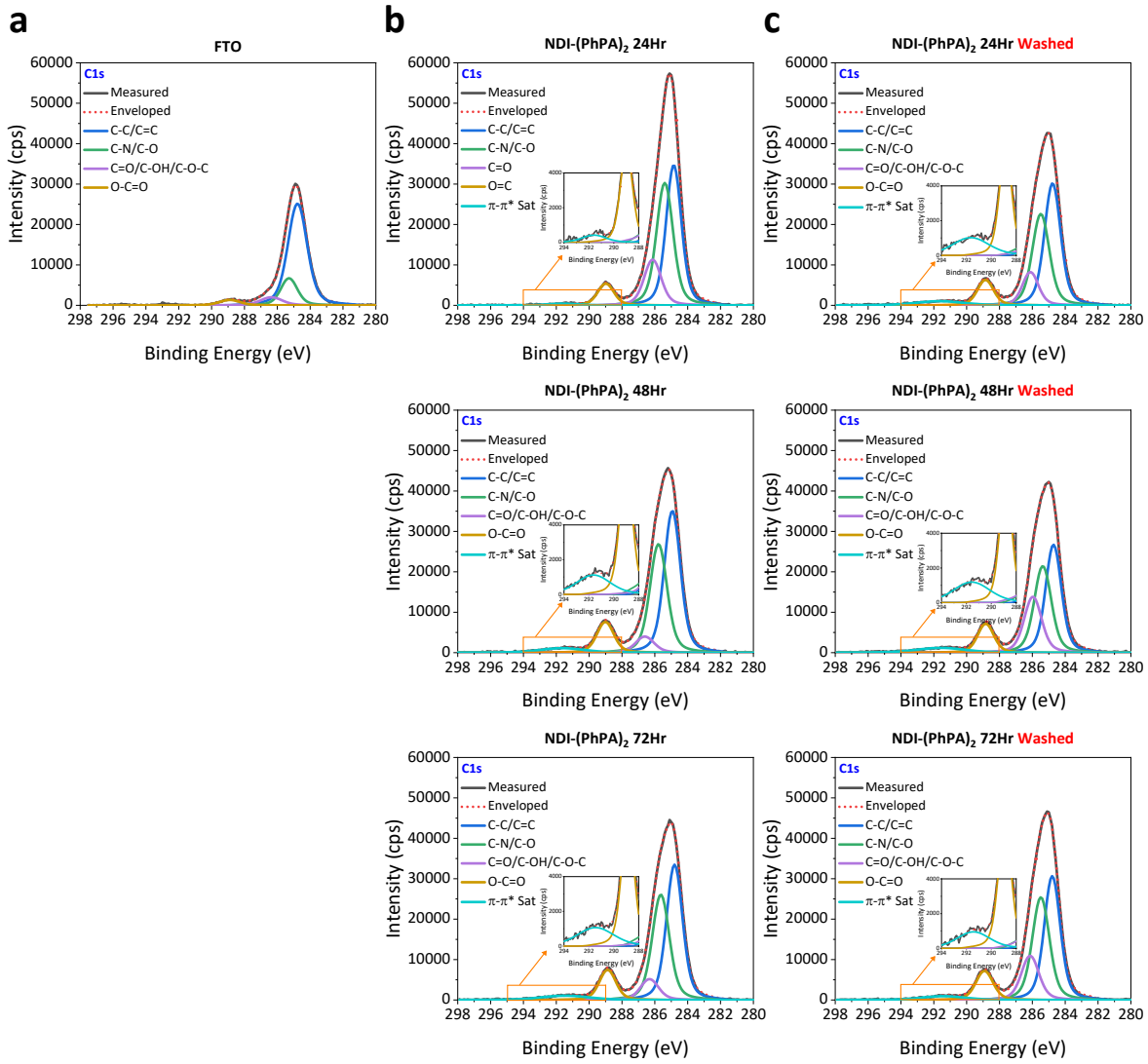

Figure S18. Surface chemistry analysis via deconvoluted XPS core level spectra of C 1s for (a) bare FTO and NDI-$(PhPA)_2$ on FTO with varying chemical durations (b) before and (c) after DMF:DMSO (2:1) + CB wash test.

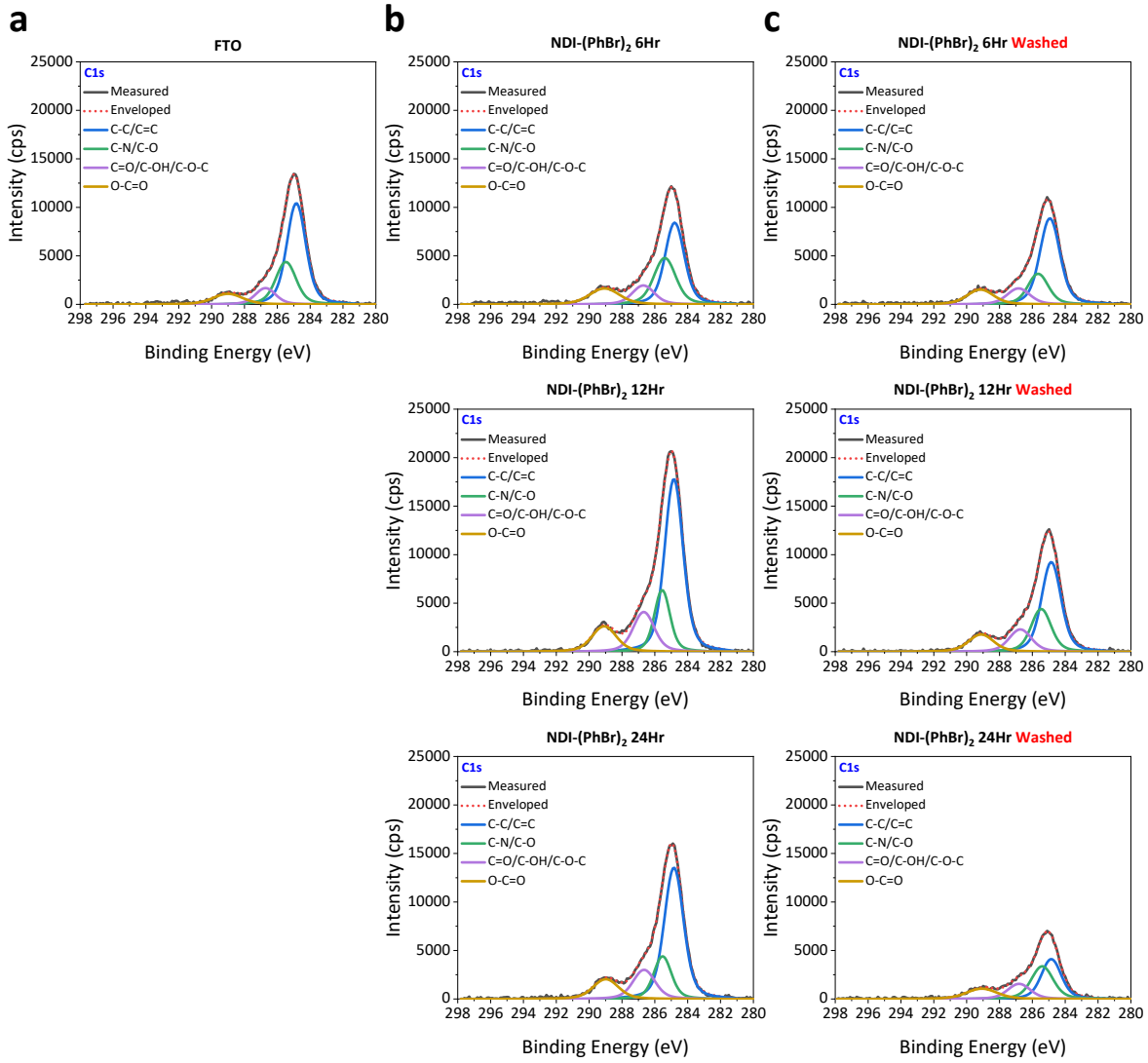

Figure S19. Surface chemistry analysis via deconvoluted XPS core level spectra of C 1s for (a) bare FTO and FTO treated with NDI-$(PhBr)_2$ CBD with varying chemical durations (b) before and (c) after DMF:DMSO (2:1) + CB wash test.

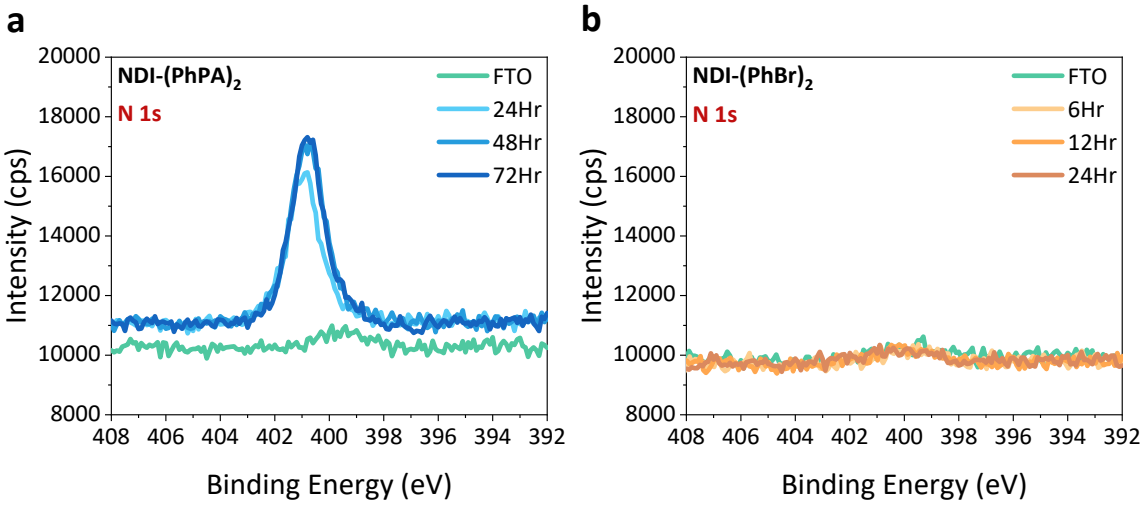

Figure S20. N 1s XPS spectra of FTO treated with (a) NDI-$(PhPA)_2$ and (b) NDI-$(PhBr)_2$ at varying CBD durations.

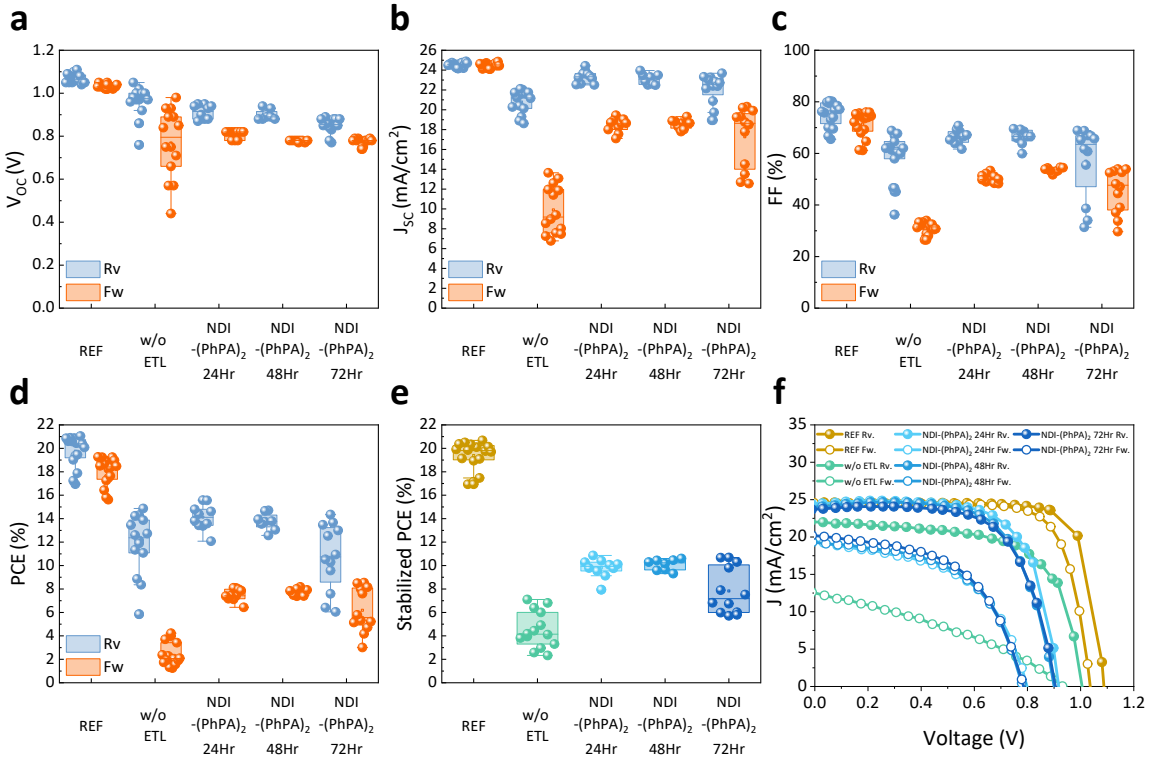

Figure S21. Statistics of (a) V_{OC}, (b) J_{SC}, (c) *FF*, (d) PCE, (e) stabilized PCE, and (f) *J-V* curves of champion devices for REF, w/o ETL, and NDI-$(PhPA)_2$ with different chemical bath durations incorporated PSCs. "REF" refers to c-TiO_2 + mp-TiO_2 and "w/o ETL" represents PSCs without an ETL.

Table S1. Summarized photovoltaic parameters for PSCs incorporating REF, w/o ETL, and NDI-$(PhPA)_2$ with different chemical bath durations.

ETL	Scan	V_{OC} (V)	J_{SC} (mA cm^{-2})	FF (%)	PCE (%)	Stabilized PCE (%)
REF	Rev.	1.07 ± 0.02	24.56 ± 0.20	75.19 ± 4.91	19.76 ± 1.34	19.38 ± 1.20
	Fwd.	1.03 ± 0.01	24.50 ± 0.21	71.31 ± 5.08	18.01 ± 1.20	
w/o ETL	Rev.	0.96 ± 0.07	20.77 ± 1.18	58.75 ± 9.48	11.83 ± 2.59	4.49 ± 1.55
	Fwd.	0.77 ± 0.16	9.93 ± 2.42	31.15 ± 2.16	2.42 ± 1.00	
NDI-$(PhPA)_2$ 24Hr	Rev.	0.91 ± 0.03	23.31 ± 0.63	66.38 ± 2.73	14.13 ± 1.08	9.79 ± 0.81
	Fwd.	0.81 ± 0.02	18.44 ± 0.71	50.31 ± 1.68	7.50 ± 0.52	
NDI-$(PhPA)_2$ 48Hr	Rev.	0.90 ± 0.02	23.09 ± 0.55	66.30 ± 3.21	13.75 ± 0.72	10.07 ± 0.48
	Fwd.	0.78 ± 0.00	18.55 ± 0.49	53.56 ± 0.97	7.74 ± 0.30	
NDI-$(PhPA)_2$ 72Hr	Rev.	0.85 ± 0.04	22.11 ± 1.49	57.03 ± 14.08	10.70 ± 2.86	7.83 ± 2.00
	Fwd.	0.78 ± 0.02	17.28 ± 3.04	45.46 ± 8.59	6.18 ± 1.89	

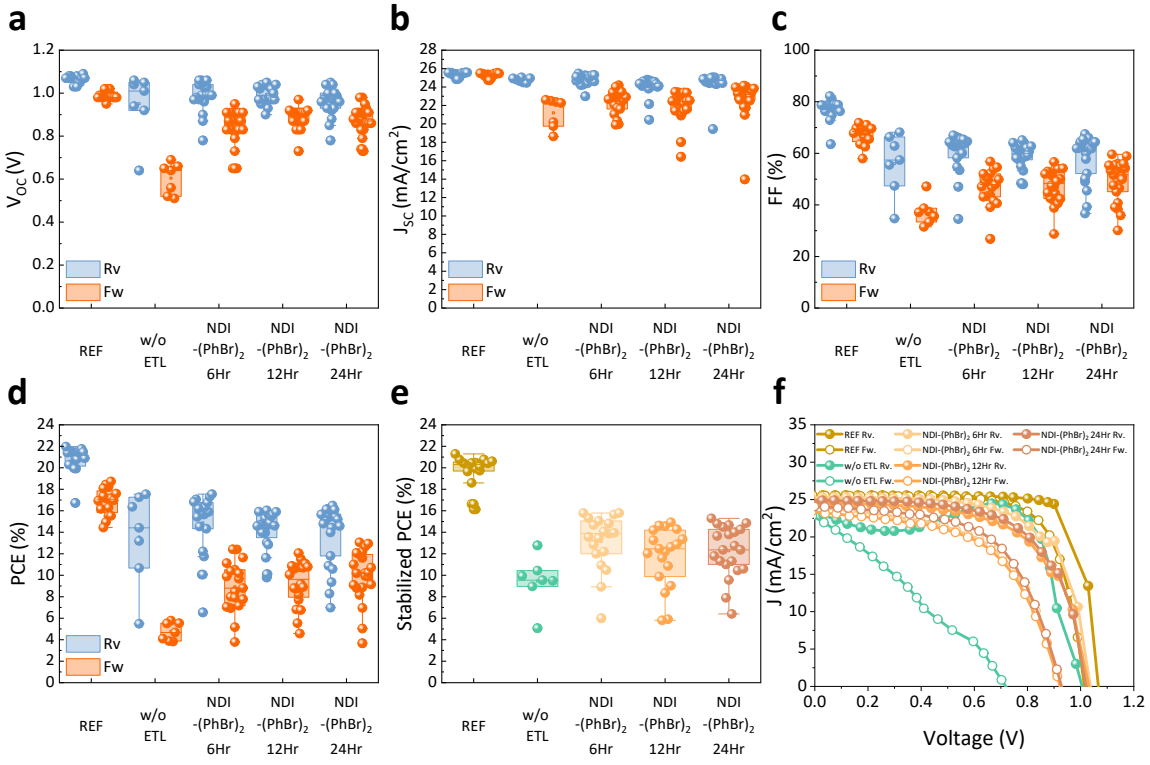

Figure S22. Statistics of (a) V_{OC}, (b) J_{SC}, (c) *FF*, (d) PCE, (e) stabilized PCE, and (f) *J-V* curves of champion devices for REF, w/o ETL, and NDI-$(PhBr)_2$ with different chemical bath durations incorporated PSCs. "REF" refers to c-TiO_2 + mp-TiO_2 and "w/o ETL" represents PSCs without an ETL.

Table S2. Summarized photovoltaic parameters for PSCs incorporating REF, w/o ETL, and NDI-$(PhBr)_2$ with different chemical bath durations.

ETL	Scan	V_{OC} (V)	J_{SC} (mA cm^{-2})	FF (%)	PCE (%)	Stabilized PCE (%)
REF	Rev.	1.06 ± 0.02	25.36 ± 0.24	77.01 ± 4.26	20.76 ± 1.26	19.76 ± 1.45
	Fwd.	0.99 ± 0.02	25.28 ± 0.24	67.27 ± 3.74	16.85 ± 1.27	
w/o ETL	Rev.	0.95 ± 0.15	24.76 ± 0.24	56.05 ± 11.77	13.56 ± 4.32	9.46 ± 2.30
	Fwd.	0.60 ± 0.07	21.19 ± 1.63	37.25 ± 5.01	4.76 ± 0.84	
NDI-$(PhBr)_2$ 6Hr	Rev.	0.99 ± 0.07	24.80 ± 0.57	60.14 ± 8.05	14.88 ± 2.84	13.13 ± 2.58
	Fwd.	0.84 ± 0.08	22.28 ± 1.27	46.77 ± 6.93	8.91 ± 2.34	
NDI-$(PhBr)_2$ 12Hr	Rev.	0.99 ± 0.04	24.08 ± 1.03	58.91 ± 4.74	14.16 ± 1.83	11.73 ± 2.78
	Fwd.	0.88 ± 0.05	21.85 ± 1.78	47.27 ± 6.81	9.22 ± 2.08	
NDI-$(PhBr)_2$ 24Hr	Rev.	0.96 ± 0.06	24.48 ± 1.15	58.45 ± 8.94	13.86 ± 2.84	12.27 ± 2.40
	Fwd.	0.87 ± 0.06	22.69 ± 2.13	49.27 ± 7.96	9.93 ± 2.43	

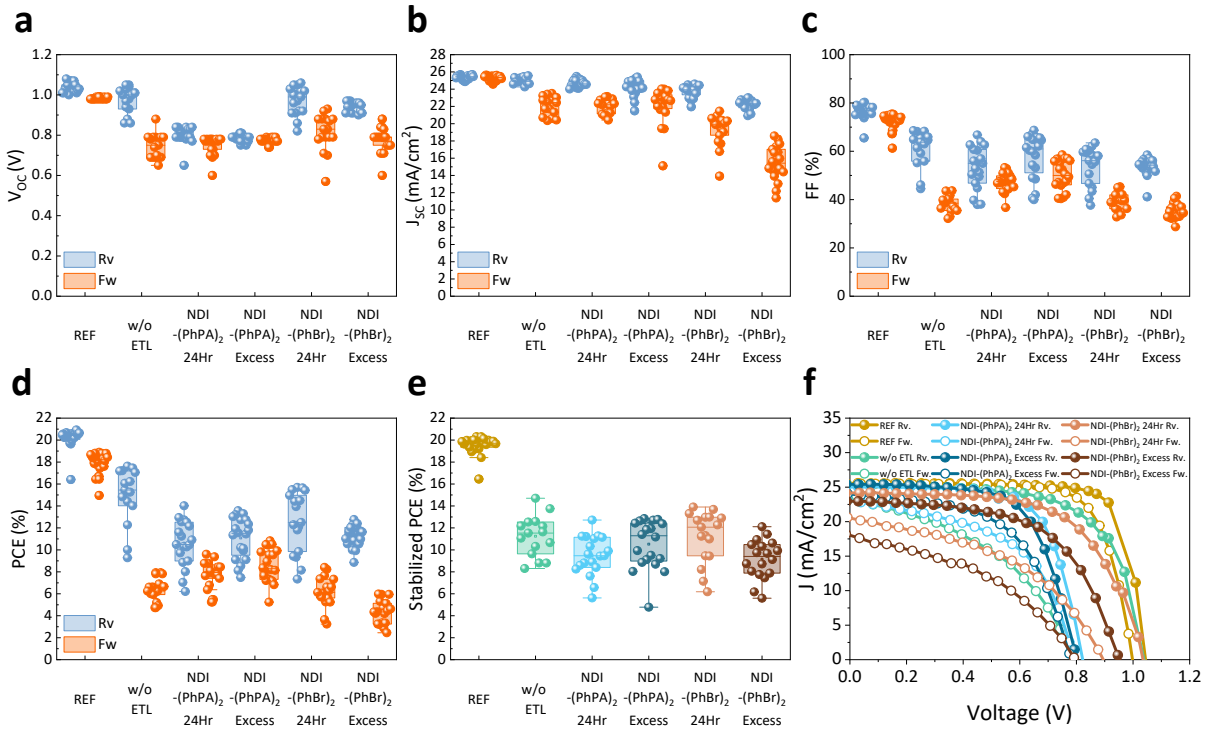

Figure S23. Statistics of (a) V_{OC}, (b) J_{SC}, (c) *FF*, (d) PCE, (e) stabilized PCE, and (f) *J-V* curves of champion devices for REF, w/o ETL, NDI-$(PhPA)_2$ 24Hr, NDI-$(PhPA)_2$ Excess, NDI-$(PhBr)_2$ 24Hr, NDI-$(PhBr)_2$ Excess incorporated PSCs. "REF" refers to c-TiO_2 + mp-TiO_2 and "w/o ETL" represents PSCs without an ETL. "Excess" denotes NDI-based ETL molecules without EtOH dipping step.

Table S3. Summarized photovoltaic parameters for PSCs incorporating REF, w/o ETL, NDI-$(PhPA)_2$ 24Hr, NDI-$(PhPA)_2$ Excess, NDI-$(PhBr)_2$ 24Hr, NDI-$(PhBr)_2$ Excess.

ETL	Scan	V_{OC} (V)	J_{SC} (mA cm^{-2})	FF (%)	PCE (%)	Stabilized PCE (%)
REF	Rev.	1.04 ± 0.02	25.34 ± 0.27	76.61 ± 2.96	20.17 ± 0.90	19.54 ± 0.85
	Fwd.	0.98 ± 0.00	25.25 ± 0.31	72.49 ± 3.23	17.98 ± 0.93	
w/o ETL	Rev.	0.97 ± 0.07	24.99 ± 0.37	61.02 ± 7.59	14.96 ± 2.62	11.24 ± 1.85
	Fwd.	0.75 ± 0.06	22.04 ± 1.14	38.20 ± 3.48	6.30 ± 0.90	
NDI-$(PhPA)_2$ 24Hr	Rev.	0.80 ± 0.04	24.70 ± 0.44	53.30 ± 8.82	10.58 ± 2.09	9.48 ± 1.78
	Fwd.	0.75 ± 0.05	21.97 ± 0.86	47.15 ± 3.93	7.80 ± 1.15	
NDI-$(PhPA)_2$ Excess	Rev.	0.79 ± 0.01	24.28 ± 1.00	57.84 ± 9.28	11.08 ± 1.88	10.52 ± 2.19
	Fwd.	0.77 ± 0.01	22.12 ± 2.10	49.98 ± 6.14	8.58 ± 1.52	
NDI-$(PhBr)_2$ 24Hr	Rev.	0.97 ± 0.07	23.72 ± 0.73	53.69 ± 8.12	12.52 ± 2.81	11.22 ± 2.34
	Fwd.	0.81 ± 0.09	19.26 ± 1.85	39.01 ± 3.78	6.18 ± 1.42	
NDI-$(PhBr)_2$ Excess	Rev.	0.94 ± 0.02	22.22 ± 0.57	53.69 ± 3.73	11.20 ± 1.01	9.16 ± 1.77
	Fwd.	0.77 ± 0.06	15.41 ± 1.98	35.15 ± 3.13	4.26 ± 1.08	

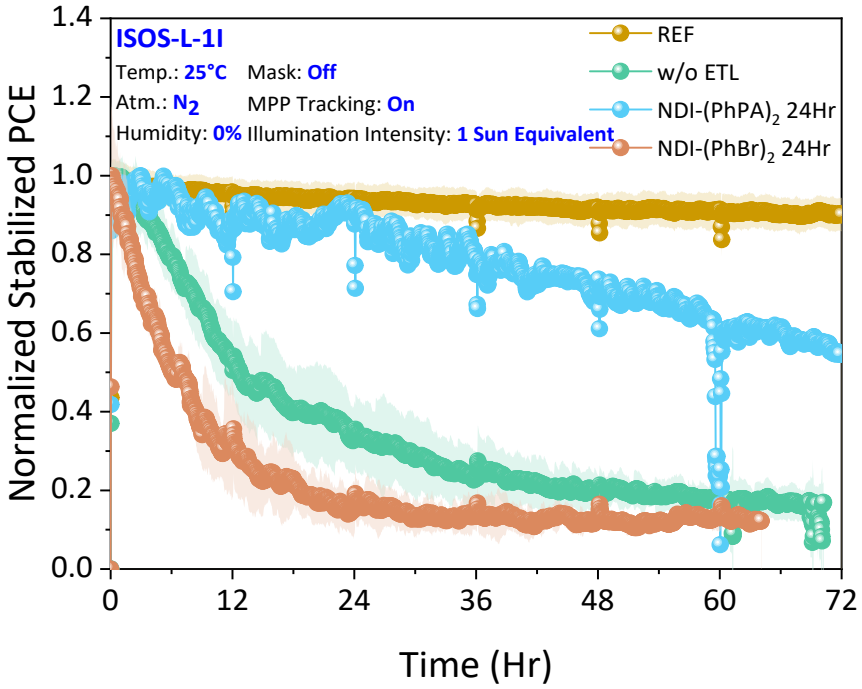

Figure S24. Normalized stabilized PCE during long-term stability measurement of REF, w/o ETL, NDI-$(PhPA)_2$ 24Hr, and NDI-$(PhBr)_2$ 24Hr. Photovoltaic parameters from *J-V* scans were automatically extracted every 12 hours during the MPPT at 25 °C. "REF" refers to c-TiO_2 + mp-TiO_2 and "w/o ETL" represents PSCs without an ETL.

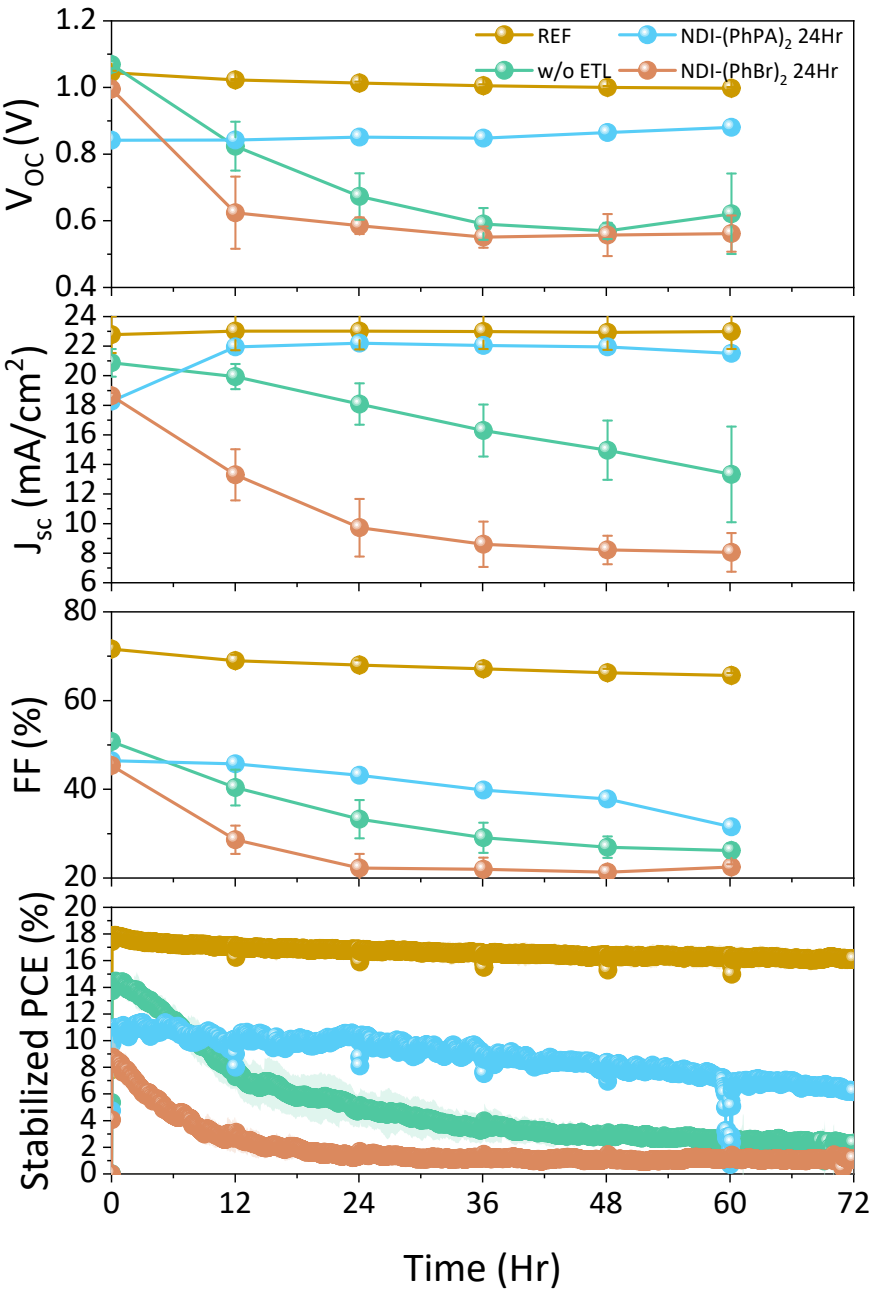

Figure S25. Evolution of the *J-V* parameters during long-term stability measurement of REF, w/o ETL, NDI-$(PhPA)_2$ 24Hr, NDI-$(PhBr)_2$ 24Hr. Photovoltaic parameters from *J-V* scans were automatically extracted every 12 hours during the MPPT at 25 °C. "REF" refers to c-TiO_2 + mp-TiO_2 and "w/o ETL" represents PSCs without an ETL.

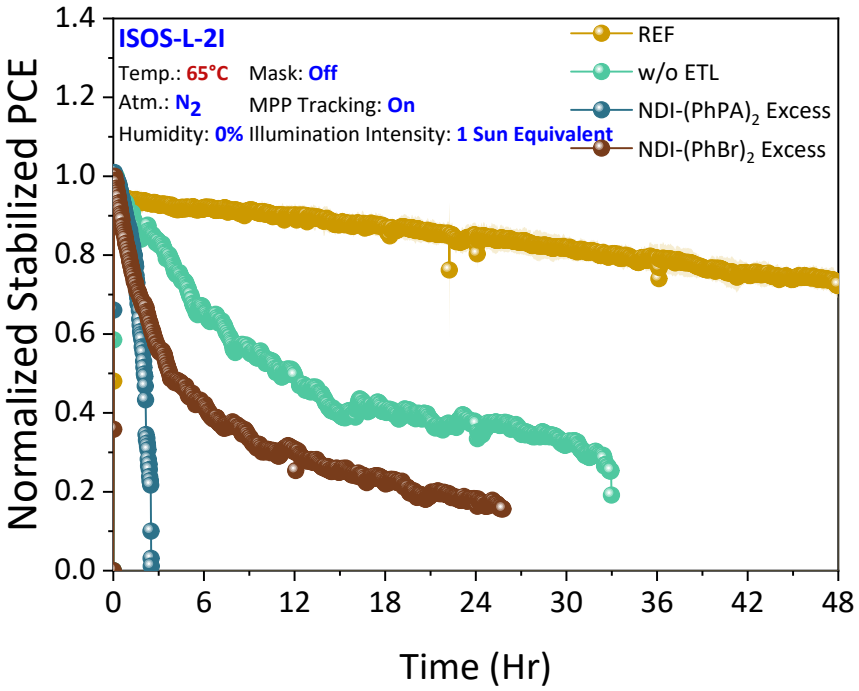

Figure S26. Normalized stabilized PCE during long-term stability measurement of REF, w/o ETL, NDI-$(PhPA)_2$ Excess, and NDI-$(PhBr)_2$ Excess. Photovoltaic parameters from *J-V* scans were automatically extracted every 12 hours during the MPPT at 65 °C. "REF" refers to c-TiO_2 + mp-TiO_2 and "w/o ETL" represents PSCs without an ETL.

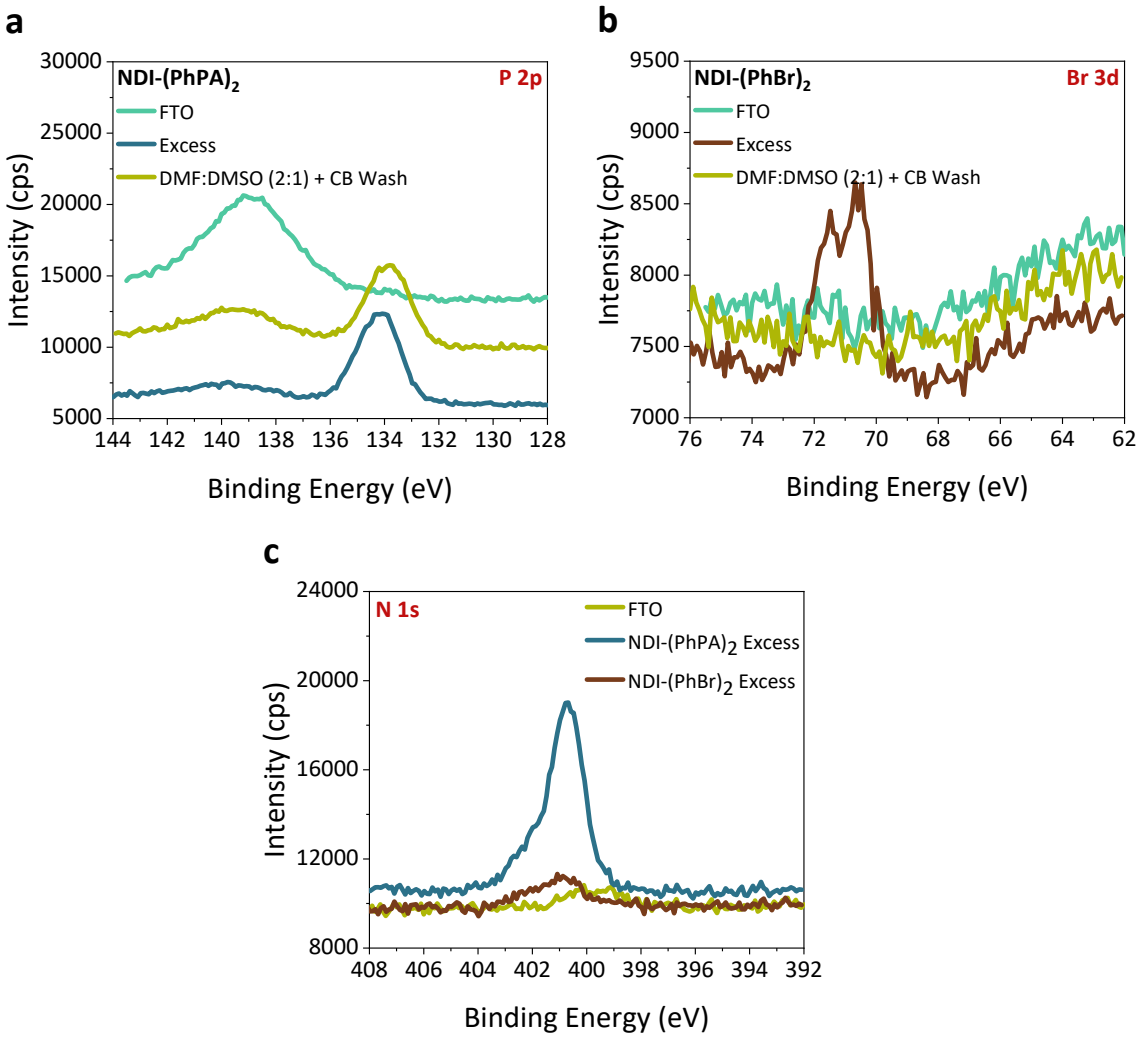

Figure S27. XPS spectra of (a) P 2p for NDI-$(PhPA)_2$ Excess and (b) NDI-$(PhBr)_2$ Excess on FTO, before and after washing with DMF:DMSO (2:1) and CB solvents, simulating the perovskite spin-coating conditions to assess molecular retention. (c) N 1s XPS spectra of NDI-$(PhPA)_2$ Excess and NDI-$(PhBr)_2$ Excess on FTO. "Excess" denotes NDI-based ETL molecules without EtOH dipping step.

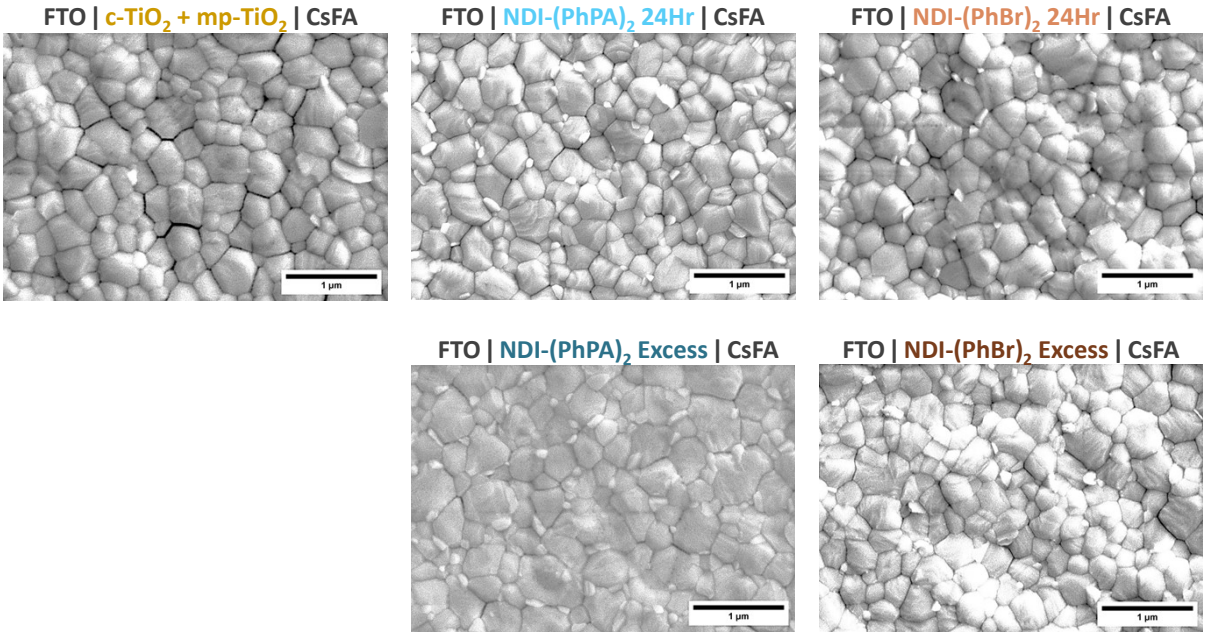

Figure S28. Top-view SEM of CsFA on c-TiO_2 + mp-TiO_2, NDI-$(PhPA)_2$ 24Hr, NDI-$(PhPA)_2$ Excess, NDI-$(PhBr)_2$ 24Hr, and NDI-$(PhBr)_2$ Excess thin films. No obvious changes in grain size were found for NDI-based ETL molecules.

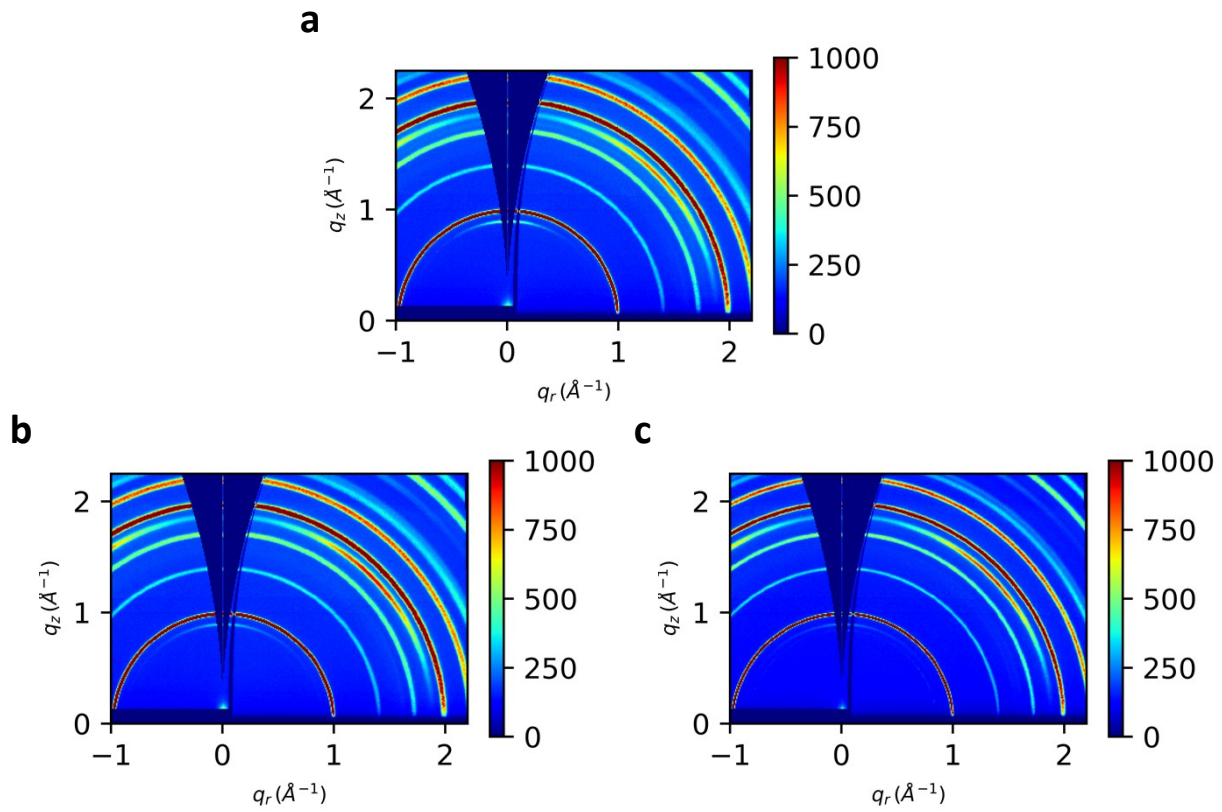

Figure S29. GIWAXS patterns of CsFA spin-coated on top of (a) c-TiO_2 + mp-TiO_2, (b) NDI-$(PhPA)_2$ Excess, and (c) NDI-$(PhBr)_2$ Excess with incident angle of 0.5°.

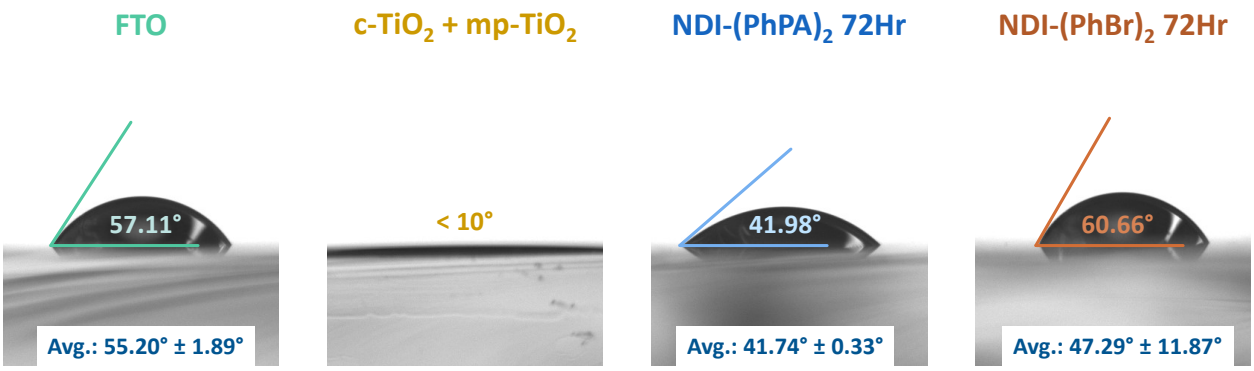

Figure S30. Water contact angle measurements on bare FTO, FTO treated with c-TiO_2 + mp-TiO_2, NDI-$(PhPA)_2$, and NDI-$(PhBr)_2$, illustrating wettability differences.

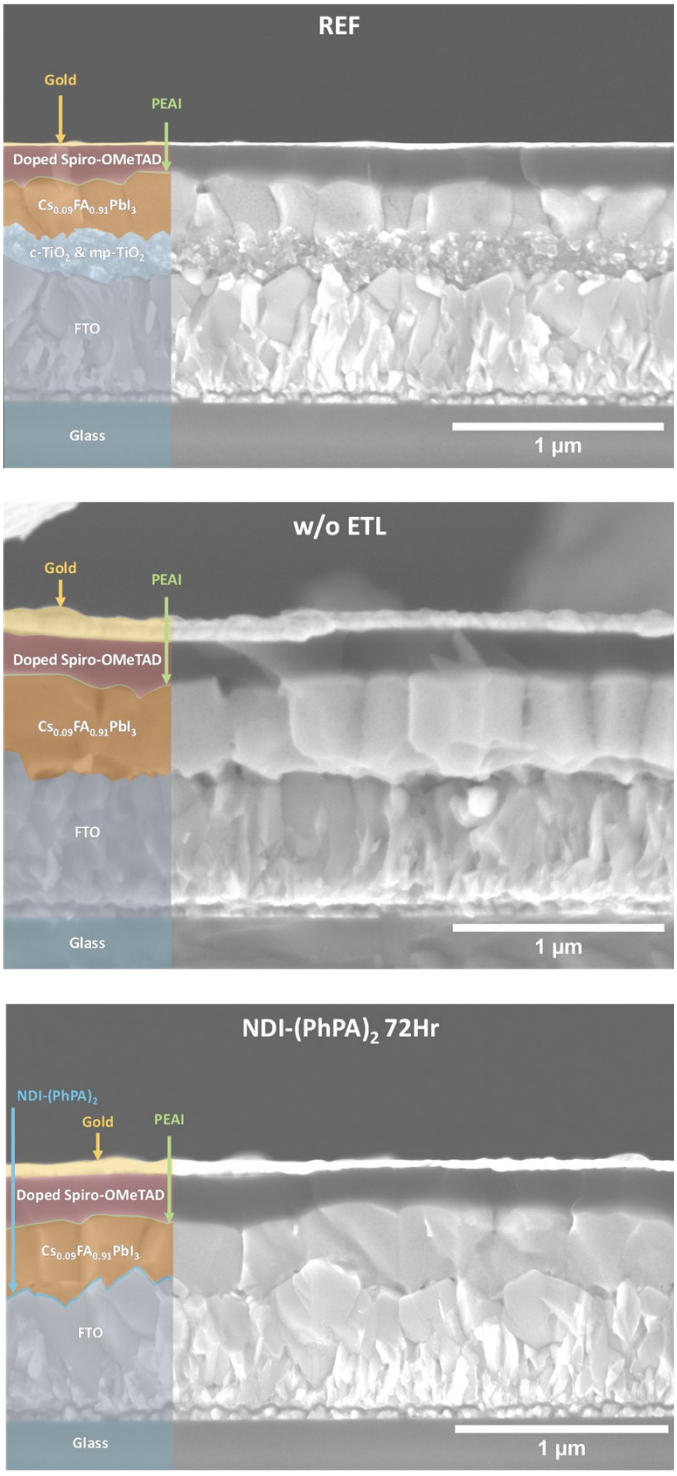

Figure S31. The cross-sectional SEM images of REF, w/o ETL, and NDI-$(PhPA)_2$ 72Hr, incorporated PSCs. "REF" refers to c-TiO_2 + mp-TiO_2 and "w/o ETL" represents PSCs without an ETL.

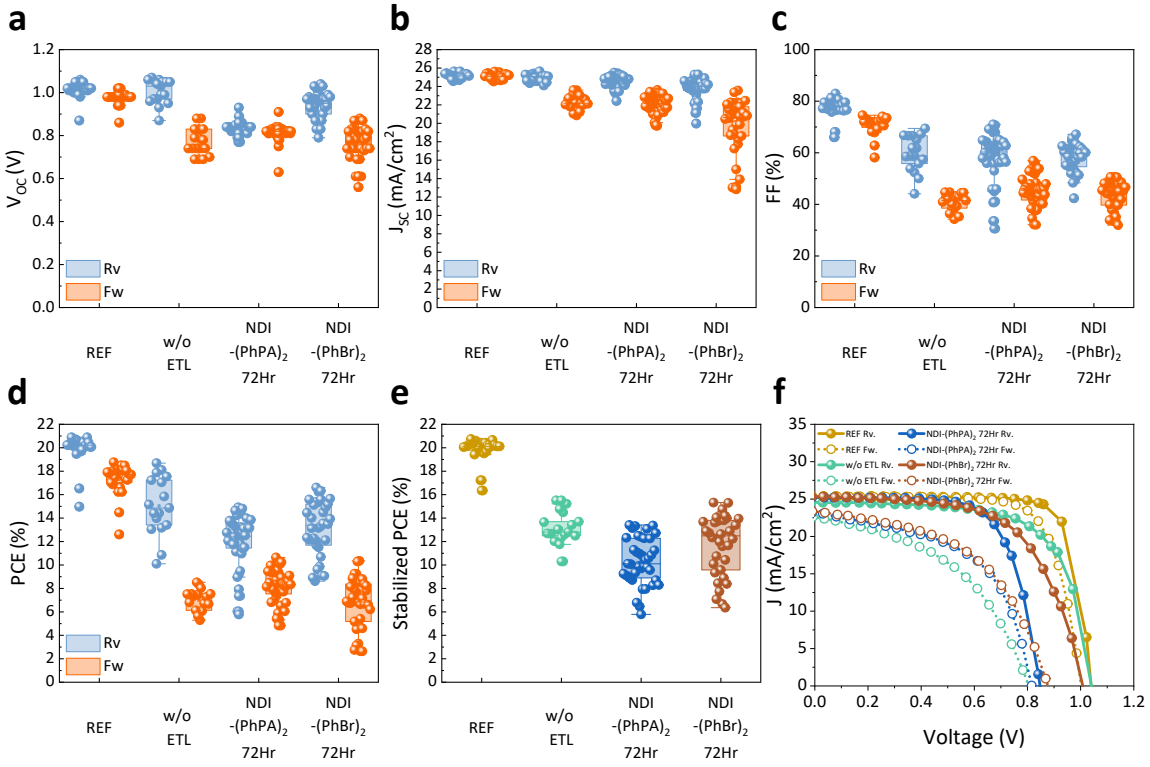

Figure S32. Statistics of (a) V_{OC}, (b) J_{SC}, (c) *FF*, (d) PCE, (e) stabilized PCE, and (f) *J-V* curves of champion devices for REF, w/o ETL, NDI-(PhPA)$_2$ 72Hr, and NDI-(PhBr)$_2$ 72Hr incorporated PSCs. "REF" refers to c-TiO$_2$ + mp-TiO$_2$ and "w/o ETL" represents PSCs without an ETL.

Table S4. Summarized photovoltaic parameters for PSCs incorporating REF, w/o ETL, NDI-(PhPA)$_2$ 72Hr, and NDI-(PhBr)$_2$ 72Hr.

ETL	Scan	V_{OC} (V)	J_{SC} (mA cm^{-2})	FF (%)	PCE (%)	Stabilized PCE (%)
REF	Rev.	1.02 ± 0.04	25.12 ± 0.29	77.65 ± 3.66	19.87 ± 1.31	19.86 ± 0.99
	Fwd.	0.98 ± 0.03	25.09 ± 0.29	70.60 ± 3.55	17.32 ± 1.34	
w/o ETL	Rev.	1.00 ± 0.06	24.93 ± 0.44	59.71 ± 7.00	15.05 ± 2.51	13.15 ± 1.33
	Fwd.	0.77 ± 0.06	22.24 ± 0.84	40.84 ± 0.84	7.00 ± 0.93	
NDI-(PhPA)$_2$ 72Hr	Rev.	0.84 ± 0.03	24.60 ± 0.64	58.27 ± 9.68	12.03 ± 2.29	10.32 ± 2.01
	Fwd.	0.81 ± 0.04	22.09 ± 0.98	45.15 ± 6.04	8.17 ± 1.44	
NDI-(PhBr)$_2$ 72Hr	Rev.	0.94 ± 0.06	23.78 ± 1.20	58.19 ± 5.56	13.10 ± 2.38	11.62 ± 2.56
	Fwd.	0.76 ± 0.08	19.67 ± 2.30	43.34 ± 5.73	6.73 ± 2.17	

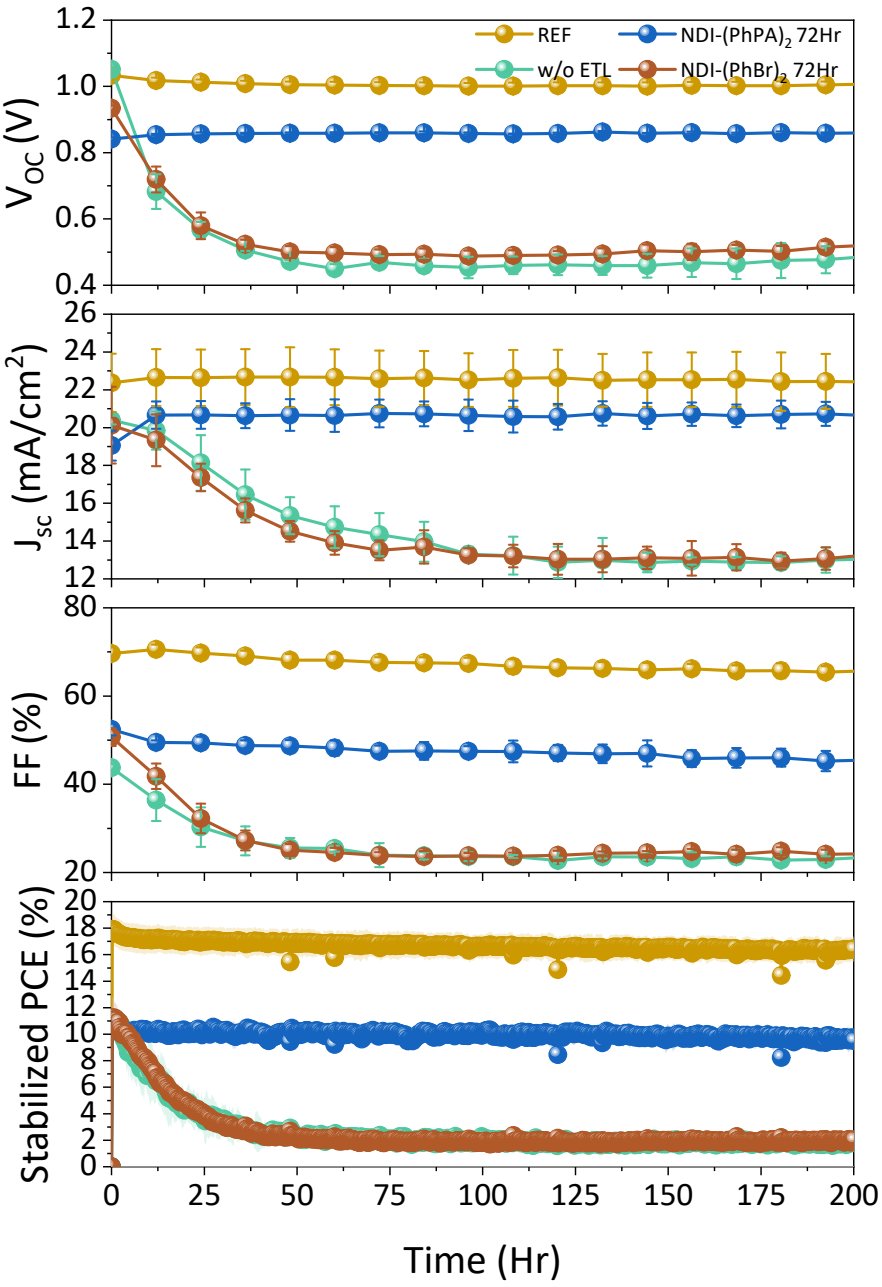

Figure S33. Evolution of the *J-V* parameters during long-term stability measurement of REF, w/o ETL, NDI-(PhPA)$_2$ 72Hr, NDI-(PhBr)$_2$ 72Hr. Photovoltaic parameters from *J-V* scans were automatically extracted every 12 hours during the MPPT at 25 °C. "REF" refers to c-TiO_2 + mp-TiO_2 and "w/o ETL" represents PSCs without an ETL.

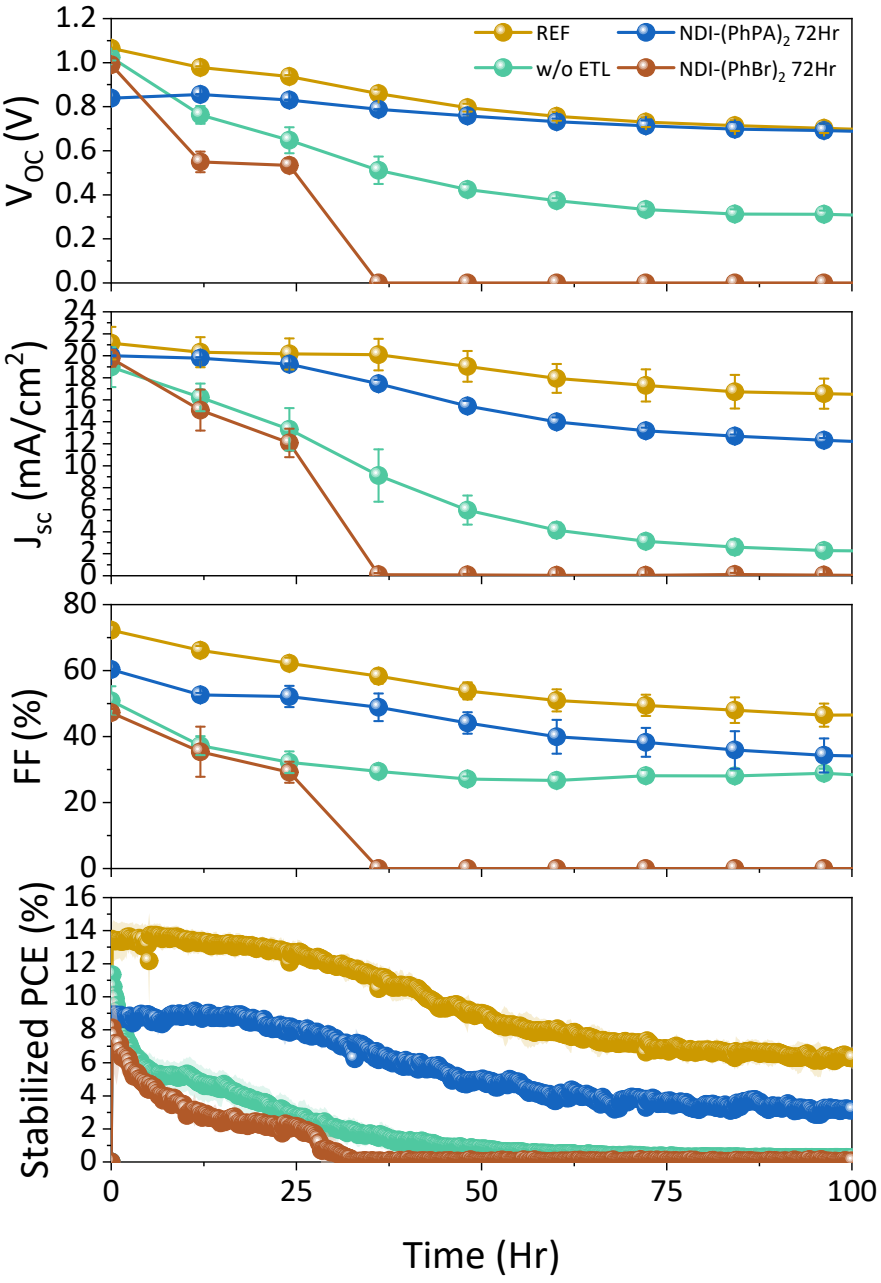

Figure S34. Evolution of the *J-V* parameters during long-term stability measurement of REF, w/o ETL, NDI-$(PhPA)_2$ 72Hr, NDI-$(PhBr)_2$ 72Hr. Photovoltaic parameters from *J-V* scans were automatically extracted every 12 hours during the MPPT at 65 °C. "REF" refers to c-TiO_2 + mp-TiO_2 and "w/o ETL" represents PSCs without an ETL.

References

1 H. Huang, J. Denne, C. H. Yang, H. Wang and J. Y. Kang, *Angewandte Chemie International Edition*, 2018, **57**, 6624–6628.

2 J. Hohnsen, L. Rryci, D. Obretenova, J. Friedel, S. Jouchaghani and A. Klein, *Molecules*, 2024, **29**, 3680.

3 M. V. Khenkin, E. A. Katz, A. Abate, G. Bardizza, J. J. Berry, C. Brabec, F. Brunetti, V. Bulović, Q. Burlingame, A. Di Carlo, R. Cheacharoen, Y. B. Cheng, A. Colsmann, S. Cros, K. Domanski, M. Dusza, C. J. Fell, S. R. Forrest, Y. Galagan, D. Di Girolamo, M. Grätzel, A. Hagfeldt, E. von Hauff, H. Hoppe, J. Kettle, H. Köbler, M. S. Leite, S. (Frank) Liu, Y. L. Loo, J. M. Luther, C. Q. Ma, M. Madsen, M. Manceau, M. Matheron, M. McGehee, R. Meitzner, M. K. Nazeeruddin, A. F. Nogueira, Ç. Odabaşı, A. Osherov, N. G. Park, M. O. Reese, F. De Rossi, M. Saliba, U. S. Schubert, H. J. Snaith, S. D. Stranks, W. Tress, P. A. Troshin, V. Turkovic, S. Veenstra, I. Visoly-Fisher, A. Walsh, T. Watson, H. Xie, R. Yıldırım, S. M. Zakeeruddin, K. Zhu and M. Lira-Cantu, *Nature Energy 2020 5:1*, 2020, **5**, 35–49.

4 A.-F. Castro-Méndez, F. Jahanbakhshi, D. K. LaFollette, B. J. Lawrie, R. Li, C. A. R. Perini, A. M. Rappe and J.-P. Correa-Baena, *J Am Chem Soc*, 2024, **146**, 18459–18469.

5 C. Bi, Q. Wang, Y. Shao, Y. Yuan, Z. Xiao and J. Huang, *Nature Communications 2015 6:1*, 2015, **6**, 1–7.